Heliophysics Senior Review 2015

The Reuven Ramaty
High Energy Solar Spectroscopic Imager
(RHESSI)

Samuel Krucker, Principal Investigator

Brian Dennis, Mission Scientist

Albert Shih, Deputy Mission Scientist

Manfred Bester, Director of Operations

Table of Contents

EXECUTIVE SUMMARY

RHESSI has provided diagnostic observations of high-energy processes in solar flares for over 13 years since its launch in February 2002. These observations address the key Heliophysics goal of understanding the fundamental processes of particle acceleration and energy release in solar eruptions, both flares and coronal mass ejections (CMEs).

RHESSI is designed for imaging spectroscopy of hard X-ray (HXR) and gamma-ray continua emitted by energetic electrons, and gamma-ray lines produced by energetic ions. The single instrument makes imaging and spectroscopy measurements with a few arcsecond angular resolution and one- to a few- keV energy resolution at energies from soft X-rays to gamma-rays (3 keV to 17 MeV). **No other current or planned observatory has this ability to provide direct quantitative information on the energetic electrons and ions that carry such a predominant part of the released energy in a flare.**

Over 102,000 events are included in the RHESSI Flare List. More than 18,000 of them have detectable emission above 12 keV, 318 above 50 keV, 89 above 100 keV, and 41 above 300 keV; 27 events show gamma-ray line emission. All the data and the analysis software have been made immediately available to the scientific community. This has resulted in **over 1,000 refereed papers** published to date that utilize RHESSI observations, with **over 200 in the two years since the last Senior Review** and a total of well over **4,000 citations per year**.

The value of future RHESSI observations is now greatly enhanced by improved complementary observations compared with those available during the first eight years of RHESSI's operational lifetime. Groundbreaking observations of thermal plasmas, magnetic fields, and heliospheric effects are now being provided on a regular basis by instruments on the Solar Dynamics Observatory (SDO), Hinode, STEREO, the Interface Region Imaging Spectrograph (IRIS), and other components of the Heliophysics System Observatory (HSO). Instruments on the Fermi astrophysics mission are providing X-ray and gamma-ray spectroscopy (with limited imaging and modest energy resolution) from ~10 keV to GeV energies. New and upgraded ground-based radio and optical facilities are becoming available to provide imaging spectroscopy data that give a complementary perspective on the energetic electrons and heated plasma deduced from RHESSI's X-ray observations.

No other instrument currently operating or scheduled for flight can provide high-resolution X-ray and gamma-ray imaging spectroscopy. Thus, **RHESSI remains an essential component of HSO**. Interpretation of data from RHESSI, especially in conjunction with data from other instruments and predictions of theoretical flare models, forms a key part of "*developing a comprehensive scientific understanding of the fundamental physical processes that control our space environment and that influence our Earth's atmosphere.*"

In the past three years we have notably used RHESSI data to challenge the basic thick-target model, dating from the 1970s and heretofore the essential description of the dominant nonthermal processes in the impulsive phase of a flare. We find evidence for bulk acceleration in the corona, and, unexpectedly, the presence of non-thermal particles in the lowest layer of the solar atmosphere, close to the photosphere itself. We anticipate major revisions in this paradigm, made possible now by the new complementary data becoming available.

The RHESSI spacecraft and instrument continue to operate well. The mission has no expendables and reentry is not predicted to occur until 2021. The slowly rising detector temperature resulting from the gradually decreasing cryocooler efficiency is not expected to be a problem until 2017 at the earliest. The germanium detectors have been annealed four times to remove most of the effects of radiation damage although with some temporary detector de-segmentation that does not affect RHESSI's core hard X-ray imaging spectroscopy capability.

1 SCIENCE AND SCIENCE IMPLEMENTATION

1.1 Prioritized Science Goals (PSGs) – Progress to Date

RHESSI's design was optimized for its primary science goal of understanding solar flare energy release and particle acceleration. In the 2013 Senior Review proposal, this overall goal was broken down into the following four major components: (1) the evolution of solar eruptive events (SEEs), (2) the acceleration of electrons, (3) the acceleration of ions, and (4) the origin of the thermal plasma. These solar flare goals were followed in our PSG list by other scientific objectives derived from RHESSI's serendipitous capabilities for making scientifically important observations of (5) the optical Sun and (6) X-ray and gamma-ray sources of both terrestrial and astrophysical origin. In this section, we outline the important progress that has been made in the last two years for each of these six goals. In Section 1.2 we discuss how new observations made with RHESSI in the coming years can further these goals.

Thirteen years of near-continuous operation have brought RHESSI into a new era of observational success. The solar maximum of Cycle 24 has been observed by an unprecedented array of space missions and other facilities, for which RHESSI provides its unique X-ray and gamma-ray imaging spectroscopy. A detailed description of the RHESSI mission, instrument, and software is given in the first six papers of the Nov. 2002 issue of *Solar Physics* (210, pp. 3–124). Briefly, it is a whole-Sun imager with high spectral and spatial resolution for the energy range from 3 keV to 17 MeV. More detail is provided in Section 2.

RHESSI hard X-ray observations have shown that the flare-accelerated electrons and ions are both intimately related to the magnetic restructuring associated with solar eruptive events (SEEs), and have confirmed that together they contain a large fraction of the total released energy (Emslie et al. 2012). Additionally, RHESSI's high sensitivity down to ~3 keV has allowed the highest temperature flare plasma to be located and characterized. There have been systematic studies of coronal HXR sources, both those with no footpoints and those only visible to RHESSI when the bright flare footpoints are occulted by the limb. As a result of these studies, fundamental new information has been obtained on the energy release, electron and ion acceleration, and plasma heating processes in flares.

RHESSI has also made fundamental discoveries in other areas of solar, terrestrial, and astrophysical studies. RHESSI's solar aspect system (SAS) has provided the best global measurements of the large-scale structure of the solar photosphere (e.g., the solar oblateness) ever obtained, opening up new areas of research that relate to the nature of the solar cycle now and in the future. RHESSI's discovery that Terrestrial Gamma-Ray Flashes (TGFs) commonly extend up to >~20 MeV has revitalized the study of these lightning-related high-energy phenomena. RHESSI also provides measurements of astrophysical high-energy phenomena such as magnetars and cosmic gamma-ray bursts.

One of the greatest strengths of the RHESSI observations lies in their complementarity with data sets from other instruments in the HSO. The relationship between RHESSI and SDO, STEREO, Hinode, and now IRIS, is symbiotic. We note also the beginning of limited solar observations with NuSTAR, EOVSA, and ALMA. These other sources provide information never before available to aid in the interpretation of RHESSI high-energy observations.

At present, we are past the maximum phase of Solar Cycle 24, and RHESSI has been detecting an average of ~5 flares per day at energies above 12 keV since 2011. Useful average rates above one such flare per day should persist through 2017. For the first time, we will have a full complement of multi-platform solar and heliospheric measurements throughout a solar cycle. We can expect synergistic studies of many SEEs in the coming years using the array of instruments in the HSO, allowing for a much more insightful analysis than was possible through much of RHESSI's observations during the previous solar cycle. Historical records of activity

show that major energetic events can occur at almost any phase of the solar cycle and, furthermore, that aspects of solar activity revealed in flare/microflare occurrence patterns may help us to understand the cycle itself.

1.1.1 Science Goal 1 – Evolution of Solar Eruptive Events (SEEs)

A primary goal of heliophysics is to understand the origin and evolution of solar flares and coronal mass ejections, and the relationship between them. It is now well established that magnetic reconnection in the corona plays a central role in the physics of solar eruptive events (SEEs), in which a flare and a CME are observed together. Progress in this science goal has been very good in the last two years thanks to new joint observations by RHESSI, SDO/AIA, and various radio observatories that are showing more clearly than ever before how these events are driven and how they evolve.

1.1.1.1 *The Primary Reconnection Current Sheet*

Direct visual evidence for magnetic reconnection and the location of particle acceleration and plasma heating has been presented by Su et al. (2013) and Liu et al. (2013) for two different SEEs. This is best seen in the videos of these events in different AIA channels available at http://hesperia.gsfc.nasa.gov/rhessi3/news-and-resources/results/movies.html

Five AIA 131 Å images spanning the full hard X-ray duration of the M7.7 limb event reported by Liu et al. (2013) are shown in Figure 1 overlaid with RHESSI 6–10 keV and 25–50 keV contours. The first image shows the flare loops, brightest at their cusp-shaped peaks, with a bright feature extending upwards that appears to be a flux rope (Patsourakos et al. 2013) whose eruption is associated with the reconnection below. Two bright 6–10 keV X-ray sources appear in this frame both above and below the presumed X-type null point within the current sheet between them. Such double coronal sources seen in similar events were previously identified with the lower and upper jets associated with magnetic reconnection occurring between them. The later images continue to show the EUV loops with a bright peak and the near co-spatial main coronal X-ray source first rising to a higher altitude, then falling, and finally rising again as the flare progresses. The image at 05:25:01 UT, the time of the hard X-ray peak, shows three 25–50 keV sources, two from the loop footpoints and one from the corona above the 6–12 keV source. This coronal hard X-ray source was investigated in detail and identified as a location of electron acceleration by Krucker & Battaglia (2014).

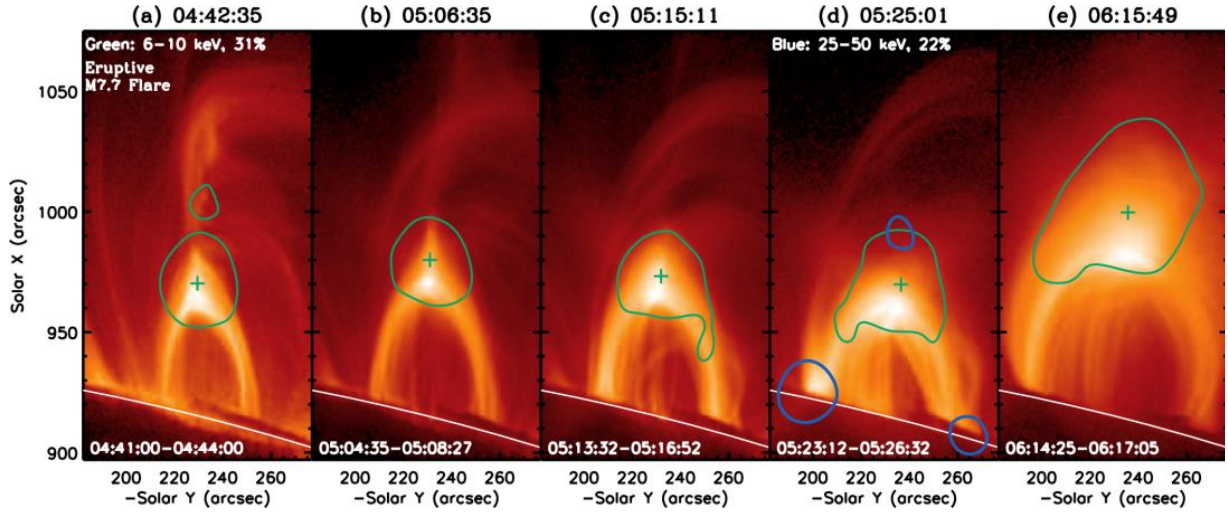

Figure 1. AIA 131 Å images for five times during the M7.7 limb event on 2012 July 19. Green and blue contours show the RHESSI X-ray sources in 6–10 and 25–50 keV energy bins, respectively.

1.1.1.2 *Quiescent Filament Eruptions*

Although quiescent filament eruptions occur outside active regions, they sometimes have the properties of SEEs but with generally weak X-ray flares. X-ray images have not previously been available to determine the location of flares that were temporally associated with filament eruptions. Thus, since Hannah et al. (2011) had shown, based on the RHESSI flare catalog, that all X-ray flares occur in active regions, it was possible that some of these were sympathetic flares in a nearby active region triggered by a filament eruption. The RHESSI observation of a compact X-ray flare co-spatial with the expanding western ribbon of a long, erupting quiescent filament and CME demonstrates that this was not the case for this event (Holman and Foord, 2015). The X-ray flare was located near a small, magnetically strong, dipolar region below the filament, but was not in a numbered NOAA active region. This discovery of X-ray flare emission in direct association with a quiescent filament eruption points to a new diagnostic of the hottest plasma that is likely to be associated with the area of most rapid energy release and the trigger of the eruption. Therefore, analysis of more events such as this should provide new insights into the physical conditions associated with the onset of filament and SEE eruptions and the conditions required for bright flares.

1.1.1.3 *SEE Global Energy Budget*

Emslie et al. (2012) used observations from a wide variety of spacecraft to study the partition of energy in 38 well-observed SEEs into various energetic components including accelerated electrons and ions, heated thermal plasma, CME, and solar energetic particles (SEPs). Studying the energy ratios of these components gives valuable clues as to the nature of the energy release and particle acceleration processes. Results from this study show that a large fraction of the released magnetic energy is manifested as accelerated electrons and ions, and that there is a general equipartition, to within an order of magnitude, between the flare and the CME energies in an SEE.

More recently, a major new project has been initiated to determine the global energetics of the 400 M- and X-class flares since the launch of SDO. As the first part of this effort, Aschwanden et al. (2014) used new magnetic field computation techniques to show that free magnetic energy in an active region varies between ~1 and ~30% of the potential energy with an average value of 10% for the 173 events they analyzed. This is to be compared to the average value of 30% that Emslie et al. (2012) had assumed for all their events. Aschwanden et al. (2015) have used AIA observations to perform a DEM analysis over a broad temperature range for all 400 events to show that the total thermal energy in the flare-heated plasma is 2-31% of the magnetically dissipated energy, an order of magnitude higher than that found by Emslie et al. (2012), who used only soft X-ray data with an isothermal plasma assumption.

1.1.1.4 *Non-thermal HXR Emissions from CMEs*

Statistical studies of RHESSI observations have shown that flare-accelerated non-thermal electrons are injected upward from the acceleration site into the escaping CME core in all eruptive flares analyzed (e.g., Krucker et al. 2008). Nevertheless, such events can rarely be observed with RHESSI because of the relatively low density of the CME core and the usual presence of intense chromospheric footpoint sources. These types of sources are therefore best seen in highly occulted flares where the main flare emissions occur behind the solar disk as in Figure 2. However, some extremely bright events exist where the emission is also seen from disk events (Bain & Fletcher 2009). The injection into the CME core is observed to be simultaneous with the injection into the footpoints, and it can occur in very large structures of up to 300 arcsec or more in extent (Krucker et al. 2007).

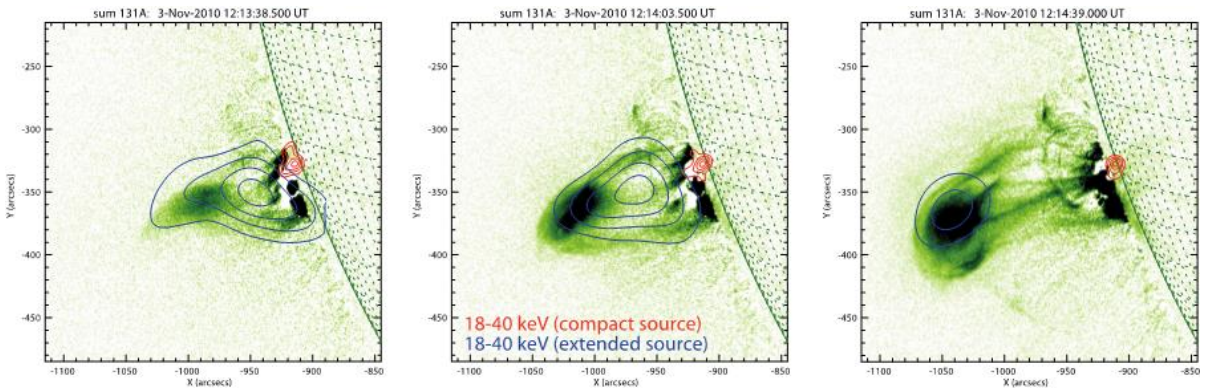

Figure 2. RHESSI and SDO/AIA 131Å imaging of an escaping CME. The three frames, taken about 30 s apart, show the escaping CME core in EUV (green image) and HXR (blue contours). The red contours show HXR emission from the top of the partially occulted flare loops.

Recent quantitative comparisons derived from joint SDO/AIA and RHESSI data, for example, show that electrons injected into the CME are responsible for heating the core of the ejected CME material by collisions, at least for the one event published so far (Glesener et al. 2013). This makes the core visible in the hot AIA channels, particularly the 131 Å channel (see Figure 2). Hence, the previously unexplained heating observed in CME material as it moves outward (e.g., Landi et al. 2010) is due to flare-accelerated non-thermal electrons as they lose their energy by collisions and heat the CME core.

1.1.2 Science Goal 2 – Flare-Accelerated Electrons

Solar flares have shown us that impulsive energy release in a magnetized cosmic plasma drastically accelerates electrons. Questions critical to understanding flares include: when, where, and how are electrons accelerated, and what happens to them afterwards? How can such a large fraction of the energy released in flares appear as energetic nonthermal electrons? Possible explanations draw both on fundamental theoretical properties of the reconnection process and on the observed properties of electron acceleration in reconnection events observed *in situ* in the solar wind, deep in the Earth's magnetotail, and in laboratory plasmas. RHESSI provides crucial information to address this question through observations of the HXR emission (predominantly electron-ion bremsstrahlung) that the accelerated nonthermal electrons produce when they interact with the ambient medium. RHESSI's X-ray imaging spectroscopy capability allows electron distributions in space and energy to be determined as functions of time during a flare.

Significant progress has been made on this science goal in the last two years thanks to new observations from RHESSI, SDO, and various radio observatories. Improved spectral analysis tools have also been introduced that incorporate various additional processes that had not previously been included such as return currents and non-uniform ionization providing a more realistic insight into electron acceleration and propagation.

1.1.2.1 *Properties of the Coronal Acceleration Region*

A recently published combined RHESSI and SDO/AIA study reports the best estimates of the ambient density within the above-the-loop-top source just before the onset of a flare. Low density values (of a few times 10^9 cm^{-3}) were found, at least 30 times lower than that of the underlying thermal flare loops (Krucker & Battaglia 2014). During the impulsive phase, the number density of accelerated electrons as derived from RHESSI spectral data was found to be of the same order, corroborating earlier findings that a bulk acceleration process energizes all electrons within the above-the-loop-top source.

Oka et al. (2013, 2015) showed that a Kappa distribution fits the HXR spectrum of an above-the-loop-top source as well as the standard power-law (Figure 3). (For theoretical work on Kappa distributions triggered by recent RHESSI results, see Bian et al. (2014)). However, the low-energy data are not well constrained and it remains an open question if the low-energy spectrum follows a Kappa distribution or a simple power law with a low-energy cutoff. The best chance to get an observation of the low-energy end is to look for occulted events where only the above-the-loop-top source is visible. We are currently searching the RHESSI database for such events.

Further theoretical work directly linked to the RHESSI observations has focused on trapping of flare-accelerated electrons. RHESSI observations clearly show that confinement of accelerated electrons is required to explain the bright coronal sources (e.g., Simões & Kontar 2013). Using the RHESSI above-the-loop-top source parameters as a starting point, new particle-in-cell (PIC) simulations (Li et al. 2014) found that electron transport is significantly suppressed by the formation of highly localized, nonlinear electrostatic potentials in the form of double layers (DLs). The formation of a DL is driven by a streaming instability due to the drift of return current electrons with respect to the ions. Energetic electrons with kinetic energies less than the electrostatic energy of the DL are therefore trapped for the DL lifetime. This mechanism provides an attractive alternative to trapping by turbulence (e.g., Chen & Petrosian 2013).

1.1.2.2 ***Electron Propagation***

Studies of the photospheric albedo emission (e.g., Dickson & Kontar 2013) have been used to infer the pitch angle distribution of the hard X-ray emitting electrons. They show that it is consistent with isotropy and that the impulsive–phase electrons do not appear to be in free-streaming highly-focused beams as assumed in the standard thick-target model. Nevertheless the thick-target model remains viable in some circumstances (e.g., Testa et al. 2014).

Codispoti et al. (2013), Gritsyk & Somov (2014), and Alaoui & Holman (2015) have studied the effect of return currents on the interpretation of RHESSI hard X-ray spectra. Alaoui & Holman applied a simple return-current model (Holman 2012) to a selection of flares with strong spectral breaks and relatively flat spectra below the break. The return current stabilizes the

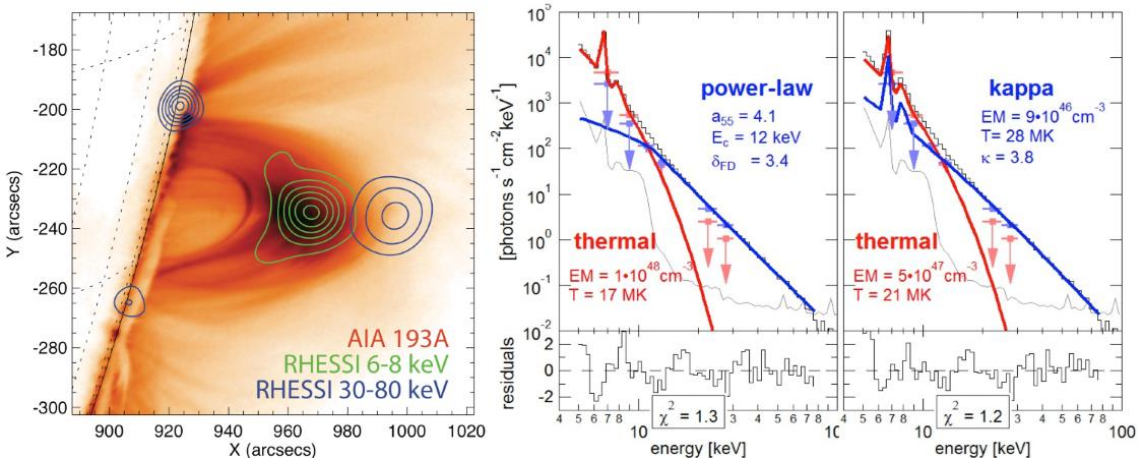

Figure 3. HXR imaging and spectroscopy of the above-the-loop-top acceleration region of the solar flare on SOL2012-07-19.. The SDO/AIA 193A image on the left show the flare loop at the western limb. The RHESSI thermal emission given in green is co-spatial with the brightest 193 A emission outlining the hottest plasma in the flare. Besides the non-thermal emission from the flare ribbons, there is also an extended coronal HXR source seen well above the flare loop. On the right, two different spectral fits to the combined coronal HXR emission is shown: the standard power law fit and the kappa distribution fit.

accelerated electrons as they stream toward the chromosphere and resupplies electrons to the acceleration region. The induced electric field that drives the return current also extracts energy from (decelerates) the streaming electrons and leads to Joule heating. The model is found in most cases to provide acceptable fits to the spectral data and also to be consistent with RHESSI and related imaging data. The results suggest resistivities of the flare plasma somewhat greater than classical (Spitzer) values, and they provide constraints on the injected electron flux density and low-energy cutoff.

1.1.2.3 *Use of Coordinated X-ray and Radio Observations*

Radio observations are an ideal complement to RHESSI HXR flare observations since they provide physically distinct perspectives on energetic electrons, hot plasma, and the magnetic field. Combining X-ray and radio observations at different wavelengths leads to important new diagnostics as follows:

- Electron spatial, spectral, and temporal distributions can be derived independently from HXR and ***microwave*** observations (e.g. Fleishman et al. 2013). Since the HXRs are density-weighted bremsstrahlung emission, while microwaves are magnetic-field-weighted gyrosynchrotron emission from the same population of electrons, coronal magnetic field strengths during flares can, in principle, be derived at different positions along the flare loop. Estimates of the coronal magnetic field strength and its evolution during a flare are crucial for evaluating flare energy budgets, for understanding particle acceleration, and for investigating the processes involved in CME initiation.
- Observations of the ***millimeter wave*** emissions of solar flares above 200 GHz (e.g., Kaufmann et al. 2013, Raulin et al. 2014) have revealed a second component with intensities well above an extrapolation of the synchrotron spectrum seen at lower frequencies. Surprisingly, the measurements at two frequencies suggest that the spectrum of this new component increases with increasing frequency in contrast to the microwave synchrotron spectrum. This exciting new finding has prompted many suggested explanations (e.g., Fleishman & Kontar 2010, Krucker et al. 2013) but the emission mechanism of this new component remains unidentified.
- Low-frequency ***decimeter-wave*** and ***meter-wave*** observations generally show coherent emission from energetic electrons associated with escaping electron beams, plasmoid ejecta, and CMEs (e.g., Battaglia & Benz 2009, Reid et al. 2014). Coherent radio bursts emitted at around the local plasma frequency provide complementary diagnostics to RHESSI HXR observations to study electron acceleration.

  The extended VLA provides imaging spectroscopy above 500 MHz allowing radio emission to be imaged from lower altitudes (higher density) giving us the opportunity to image decametric emission for the first time. The most essential context observations for EVLA are RHESSI HXR imaging spectroscopy. The first results of combined RHESSI and EVLA observations were reported by Chen et al. (2013). They reveal the trajectory of escaping electron beams relative to the flare site seen by RHESSI. The electron beams were observed to originate from a large number of over-dense and ultra-thin (>100 km) loops revealing that the localized energy release is highly fragmentary in time and space.
- Of the many types of **decametric** radio bursts, decametric spike bursts are of particular interest as they are thought to be a direct radio signature of the acceleration process itself. Combined RHESSI and VLA images shown in Figure 4 from Chen et al. (2014) reveal that the decametric spike bursts are indeed co-spatial with a non-thermal HXR source in the corona. Furthermore, the ambient density, and hence also the plasma frequency, derived from the RHESSI observations confirmed that the spike bursts were indeed fundamental plasma emission.

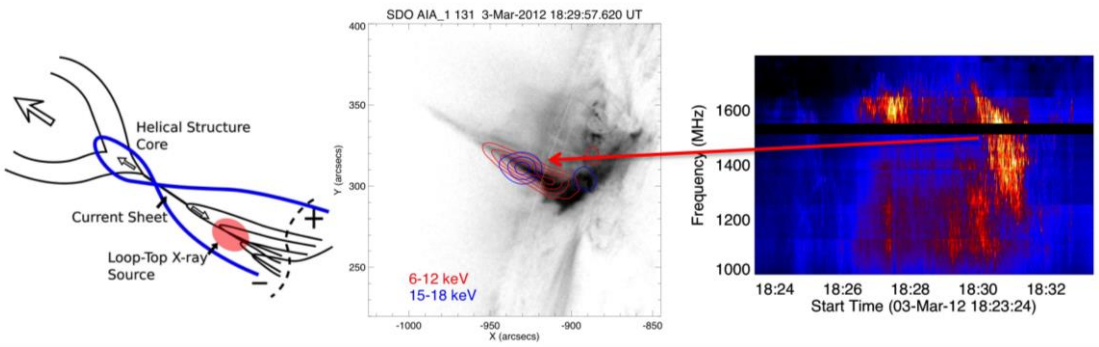

Figure 4. Eruptive event with decametric spike bursts observed by the EVLA and RHESSI: The central figure with RHESSI contours on an AIA 131 Å image shows the elongated loop structure at 6-12 keV and the nonthermal loop-top HXR source at 15-18 keV, as outlined in the cartoon on the left. The temporal and spectral variation of the radio emission from the location of the nonthermal HXR source reveals spike bursts in the righthand figure.

1.1.3 Science Goal 3 – Flare-accelerated Ions

There can be comparable energy content in flare-accelerated ions and flare-accelerated electrons (e.g., Emslie et al. 2012), and thus understanding the role of ions in flares is critical. The nuclear de-excitation lines, the positron-annihilation line at 511 keV, and the neutron-capture line at 2.223 MeV in flares reflect the composition, spectrum, and angular distribution of the accelerated ions, and also the density and composition of the solar atmosphere in which the ions interact. RHESSI provides measurements of all of these gamma-ray spectral features for the largest and most energetic solar flares, and it has observed the neutron-capture line in tens of flares.

Progress in this science goal over the last two years has been limited by the absence of the most intense gamma-ray line flares during this relatively weak solar cycle. The biggest flare observed by RHESSI in this cycle was an X4.9 flare on 09 August 2011 but it did not produce sufficient intensity in the 2.2 MeV neutron-capture line to allow for statistically useful imaging. However, exciting new advances have been made on two types of gamma-ray events: over-the-limb events with gamma-ray sources covering a large area on the visible disk, and the events discovered with the Large Area Telescope (LAT) on Fermi with >100 MeV gamma-ray emission lasting for several hours. In addition, a new method (Torre et al. 2015) allows proton spectra to be determined from the gamma-ray data without any prior assumption about the distribution. Most notably, it has now been found that excellent gamma-ray spectra can also be obtained from RHESSI's front segments.

1.1.3.1 *Location and Extent of Gamma-ray Source(s)*

RHESSI has produced the only high-resolution imaging of flare gamma rays (Hurford et al. 2003, 2006). The gamma-ray sources of the 2.223 MeV neutron capture line showing where ions stop in the atmosphere were found to be separated by up to tens of Mm from the bremsstrahlung HXR sources that reveal where accelerated electrons stop. This result strongly suggests distinct acceleration processes for the ions and electrons. Flares that produce sufficient gamma-ray emission for such imaging studies are rare, and even a single additional flare can further develop these remarkable results.

Recently, both RHESSI and Fermi/GBM, observed unusual solar gamma-ray emission during SOL2014-09-01 (Krucker et al., in preparation). RHESSI imaging data reveal the presence of an extended X-ray source associated with an occulted flare. The observations show that a significant fraction of the >50 keV X-ray emission came from angular scales greater than

the 3 arcminutes of RHESSI's coarsest subcollimator, suggesting that the event was similar to the over-the-limb event reported by Vestrand & Forrest (1993). Such extended X-ray emission from occulted flares imply electron trapping in extended coronal structures.

1.1.3.2 *Phases of Particle Acceleration*

Fermi/LAT has detected >~100 MeV emission from tens of solar eruptive events since its launch in 2008 (Ackermann et al. 2014; Ajello et al. 2014). Many of these events fall into the category of long-duration gamma-ray flares (LDGRFs) as defined by Ryan (2000), with emission persisting for many hours following the impulsive phase of the flare. While this emission is likely from the decay of pions produced by >300 MeV protons accelerated by the SEE, the time and site of the acceleration remain unknown.

RHESSI observations complement the LAT observations by providing imaging and spectroscopy for HXR and gamma-ray emission during the impulsive phase of the flare and upper limits for the sometimes hours afterwards when LAT still detects >100 MeV gamma rays. While GBM on Fermi can also provide HXR and gamma-ray spectroscopy, it has limitations: for HXR spectroscopy, its lower spectral resolution and higher threshold energy complicate discriminating thermal emission from nonthermal emission, and, for gamma-ray spectroscopy, its lower spectral resolution and instrumental background reduce its sensitivity to the narrow neutron-capture line compared to RHESSI.

Figure 5 shows RHESSI and Fermi/LAT data for the LDGRF SOL2011-03-07. Fermi was occulted by the Earth during the HXR flare but RHESSI spectroscopy provides both the energy content in flare-accelerated electrons, and an upper limits on the presence of ~30 MeV accelerated protons at the Sun. Furthermore, since LAT can only provide approximate localizations of the source of the >~100 MeV emission, RHESSI's high-resolution imaging at lower energies may be key to understanding the morphology relevant to LDGRFs.

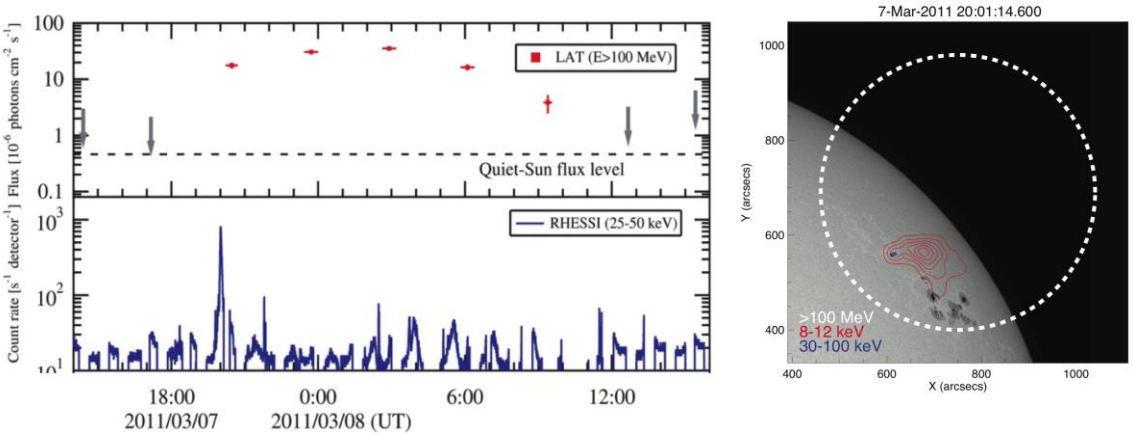

Figure 5. Left: Lightcurves of the M3.7 flare SOL2011-03-07T20:12, showing Fermi/LAT gamma-ray data and RHESSI HXR data from Ackermann et al. (2014). The >~100 MeV emission persists for half a day, long after the impulsive phase of the flare. Right: Comparison of the LAT localization (68% error) of long-duration >~100 MeV emission (white circle) compared with the high-resolution images from RHESSI during the impulsive phase showing the HXR footpoints where electrons stop (blue) and the large soft X-ray thermal source (red).

1.1.4 Science Goal 4 – Flare-heated Plasma

The hot plasma in flares appears simultaneously with flare-accelerated particles (the Neupert effect). Characterizing the temperatures and locations of flare-heated plasma reveals the partition between direct heating and collisional losses. RHESSI is sensitive to the hottest

plasmas with temperatures above ~10 MK and is also uniquely capable of determining the energy of flare-accelerated particles and *where* that energy is deposited.

Significant progress has been made in achieving this science goal over the last two years as the result of extensive coverage of events jointly observed by RHESSI and by UV and EUV instruments on SDO, Hinode, and IRIS and by ground-based optical observatories. The new results cover thermal emissions from all altitudes in the flaring solar atmosphere. Together with the energy of the accelerated electrons determined from the RHESSI HXR observations, they provide quantitative information on the origin, location, and magnitude of the heating for comparison with the predictions of ongoing theoretical and modelling efforts.

1.1.4.1 *Chromospheric Flare Plasma*

With the launch of the IRIS mission, there is a new sub-arcsecond diagnostic tool to study the response of the energy input into flare ribbons by flare-accelerated electrons as deduced from RHESSI observations. The X1 flare SOL2014-03-29 gave us an ideal set of observations with the IRIS slit crossing a HXR footpoint source during the impulsive phase (Figure 6). IRIS detected, for the first time, hydrogen recombination UV radiation resulting from the flare-accelerated electrons measured by RHESSI (Heinzel & Kleint 2014). Quantitative analysis of the same area of the flare ribbon reveals that the energy input by electrons deduced from RHESSI data is of the same order as the radiative losses inferred from IRIS in combination with other observatories. The bulk of the energy of flare-accelerated electrons heats chromospheric plasma only to low (~10,000 K) temperatures, producing high luminosity in the optical-IR range (Milligan et al. 2014, Kleint et al. 2015), at least for the few events studied in detail.

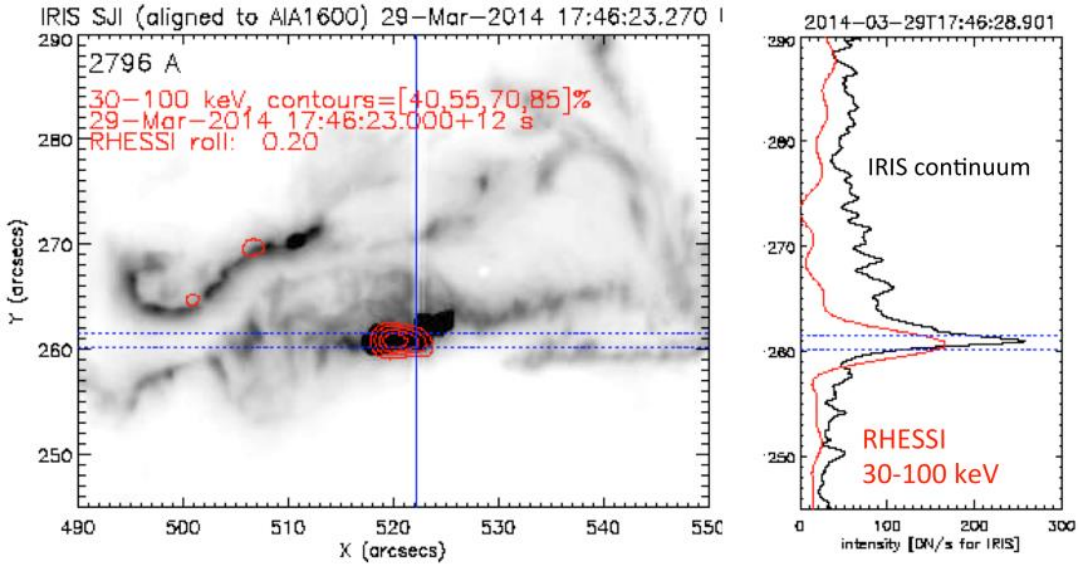

Figure 6. IRIS and RHESSI observations of the X-class flare of March 29, 2014. On the left, the IRIS slit-jaw image at 2796 Å is shown with the RHESSI 30–100 keV countours in red. The IRIS slit (solid blue vertical line) passed through the HXR source. On the right, the intensity profile along the slit is shown for the IRIS continuum enhancement (wavelengths without lines in the IRIS band) in black and for the RHESSI HXR flux in red.

IRIS also provides measurements of hot (~10 MK) plasma through the FeXXI line (Tian et al. 2014) revealing upflows of hot plasma from the flare ribbons and hot downflows from the reconnection region deduced from RHESSI imaging. We have just started comparing these upflows with the location of HXR footpoint emission to test the standard flare picture, where evaporation is caused by precipitating electrons. At the current stage, conductive evaporation or direct photospheric heating are alternative mechanisms. Initial results of the X-class flare of

SOL2014-03-29 reveal that some locations with strong upflows indeed match the HXR footpoints, but a time lag of about 1 minute is observed (Battaglia et al. 2015). Other locations with equally strong upflows, however, are not detected in HXRs, potentially indicating either that RHESSI has insufficient dynamic range to see these emissions or that a different mechanism drives the evaporation at these locations.

1.1.4.2 *White-light Continuum*

New RHESSI and SDO results establish that HXR and white light (WL) emissions from flare ribbons are co-spatial in ***all three dimensions*** (Martinez Oliveros et al. 2012, Krucker et al. 2015, see also Figure 7). Most surprisingly, both emissions originated from the same very low altitudes above the photosphere, at only a few 100 (±150) km in one event. Such low altitudes strongly restrict the parameter space for the standard thick-target beam model. Only very low ambient densities within the flare footpoints can reproduce such altitudes, especially if the HXR-producing electrons are only weakly beamed as suggested by spectral observations. To explain such low HXR source altitudes, Varady et al. (2014) proposed local reacceleration within chromospheric ribbons. For such a case, the secondary acceleration in the chromosphere allows the electrons to reach lower altitudes compared to the standard thick-target model. However, the nature of the secondary acceleration lacks observational evidence and its source of energy is problematic.

Other more indirect evidence that the energy is deposited at unexpectedly low altitudes comes from recent elemental abundance measurements of the hot flare plasma made with RESIK, RHESSI, and MESSENGER/SAX soft X-ray spectroscopic observations (Sylwester et al. 2014, Dennis et al. 2015) and from SDO/EVE observations (Warren 2014).

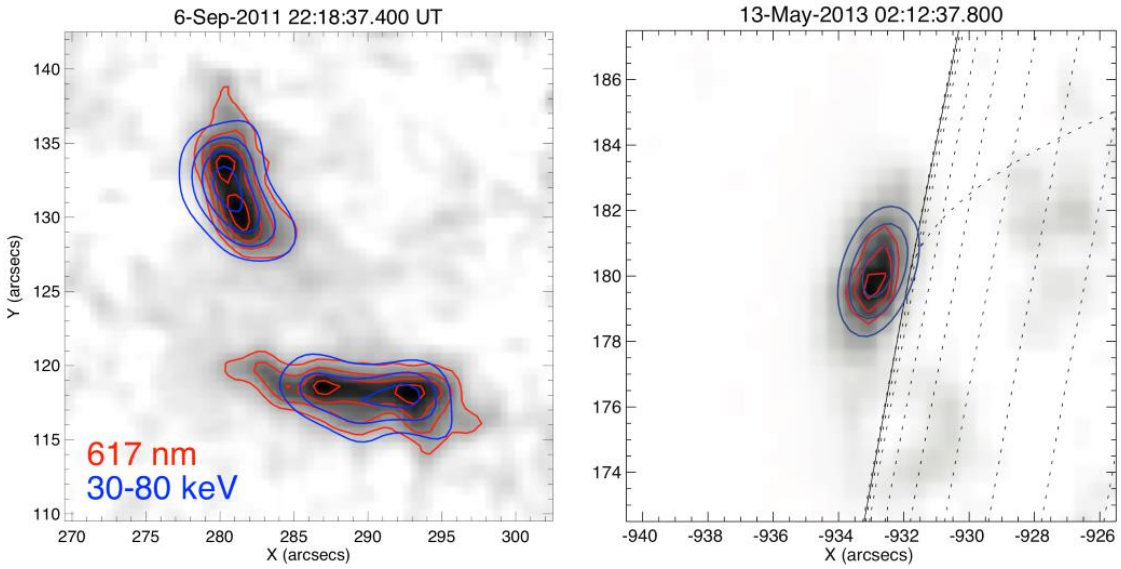

Figure 7. RHESSI and SDO/HMI observations of flare ribbons seen on the disk (left) and above the limb (right). The images show the background-subtracted HMI image with enhanced emission in dark. The contours give the RHESSI 30-100 keV hard X-ray emission in blue, and the HMI contours in red. The spatial agreement for both types of events highlights that HXR and WL emission come from the same volume.

1.1.4.3 *Infrared to mm-wave continuum*

The Halloween flares of 2003 provided the unexpected, and still unexplained, discovery of bright flare emission at the "opacity minimum" region of the solar atmosphere, 1.56 μm (Xu et al. 2004). Now we have related observations at 5 μm and 10 μm (Kaufmann et al. 2013; M. Penn,

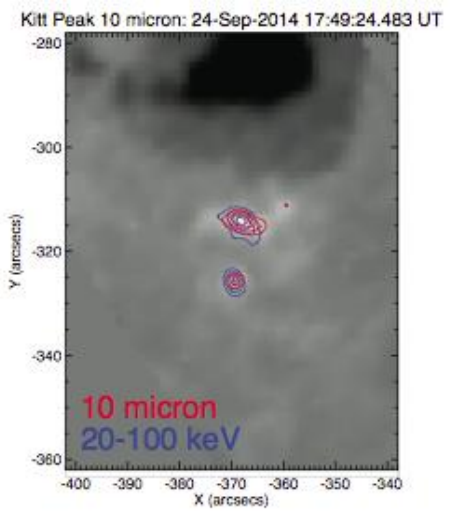

Figure 8. Preliminary view of an infrared observation of SOL2014-12-14 (C7.7) at 10 μm from the McMath telescope at NSO Kitt Peak (M. Penn, personal communication 2015). Note the close agreement of the IR and RHESSI HXR footpoint sources.

private communication 2015). The IR matches the impulsive phase and supports the RHESSI finding of powerful energy release well below the chromosphere (Martinez Oliveros et al. 2012). Figure 8 shows a very recent observation from the McMath telescope at Kitt Peak National Observatory. This exciting development inspires our proposed efforts to understand RHESSI observations in the context of these new ground-based IR and submm-mm wave (ALMA) observations.

1.1.4.4 *Computational Models*

Two different flare simulation codes are being used to predict the radiation from the solar atmosphere heated by the flare-accelerated electrons as they propagate down from the corona. These are the radiative hydrodynamic RADYN code described by Allred et al. (2005, 2015) and the HYDRAD code (Bradshaw and Cargill 2013). Both codes take the flare-accelerated electron spectra derived from RHESSI HXR observations and predict the thermal emissions for comparison with GOES, SDO, HINODE, and IRIS observations at many different wavelengths (e.g. Testa et al. 2014). By minimizing the residuals between the predicted and observed intensities and light curves, the models can be constrained and fine-tuned. As an example, Figure 9 shows an IRIS flare spectrum, which matches the blackbody and hydrogen recombination continuum spectra computed using RADYN with a range of parameters.

Not all simulations explain the observations well. For example, there are many important differences between the predicted and observed fluxes for the 15-Feb-2011 X-class solar flare

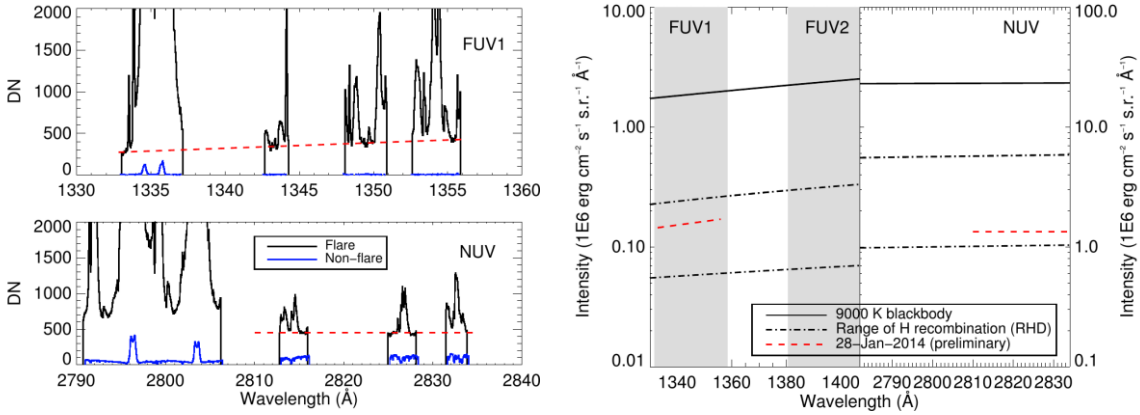

Figure 9. Left: IRIS spectra extracted from the brightest kernel in SOL2014-01-28T07:30 (M3.6) over two wavelength intervals with estimated continuum levels indicated by red dashed lines. A spectrum from a nearby non-flaring region is shown in blue. Right: The two broken black lines in each wavelength interval show a range of predicted hydrogen recombination (Balmer continuum) spectra obtained using RADYN. The red dashed lines indicate the preliminary results from the measured continuum shown in the left-hand figure after applying the radiometric conversion provided by the IRIS team. The response to a 9,000 K blackbody spectrum is shown for comparison (solid black line).

(Milligan et al. 2014). For this event, the observed Lyman-alpha line flux dominates the integrated continuum flux by approximately an order of magnitude, whereas the predictions show that the line and continuum fluxes are the same to within a factor of two. Also, the Hinode/SOT narrow-band white-light channels were observed to be more than an order of magnitude lower than the integrated He II continuum whereas the model predicts that the two fluxes are the same, again within a factor of two or so. Similar successes and difficulties have been found in comparing observations with predictions made using the HYDRAD code for the event on 25 September 2011 observed by the EIS instrument on Hinode (Doschek et al. 2015, submitted). Work is ongoing to resolve these discrepancies by adapting different parameters such as the duration of heating by non-thermal particles on individual field lines, as well as by increasing the total energy of the nonthermal electrons by lowering the cutoff energy below the upper limit provided by RHESSI.

1.1.4.5 ***Thermal Coronal Plasma***

A self-consistent flare differential emission measure (DEM) over all relevant temperatures requires a joint analysis of data from several different instruments with RHESSI providing information on the highest temperature plasma at temperatures above ~8 MK (e.g., Ryan et al. 2014). Caspi et al. (2014b) performed a joint DEM analysis on two X-class flares using both RHESSI data and SDO/EVE spectra to obtain self-consistent flare DEMs from ~2 MK to ~50 MK. Inglis & Christe (2014) demonstrated that new insights into microflare energetics can be obtained from a joint analysis of RHESSI 4–20 keV X-ray data and optically thin SDO/AIA images. They established that a steep high-temperature fall-off in DEM is required to explain joint AIA and RHESSI observations and that the nonthermal energy content in the microflares studied was substantially less than the thermal energy content, contrary to previously derived estimates based on single instruments and isothermal models.

RHESSI is also uniquely capable of characterizing so-called “super-hot” (>~30 MK) flare plasma. A survey of RHESSI flares (Caspi et al. 2014a) showed that such distinct super-hot plasmas are commonly present in association with high emission measures and high thermal energy densities, suggesting that they are physically distinct from the relatively cooler ~10–20 MK plasma. High thermal energy densities suggest that super-hot flares require strong coronal magnetic fields, exceeding ~400 G for the largest events, and that both the plasma β and the volume filling factor cannot be much less than unity in the super-hot region. Images that spatially distinguish the super-hot region from the cooler region can be produced by combining RHESSI visibilities at different X-ray energies (Caspi et al. 2015).

As a result of our joint RHESSI-SDO/HMI data analysis efforts, it was discovered that **coronal** WL flare emission (``white-light prominences'') can be detected with HMI, thus opening up new opportunities for understanding the origin of this emission. There are at least two possible mechanisms at work in producing the coronal WL emission. Some sources are seen in emission from catastrophically cooled flare loops as shown in Figure 10. Saint-Hilaire et al. (2014) showed that some sources are linearly polarized at the right orientation to be consistent with Thomson-scattered photospheric light. This opens a new diagnostic tool since Thomson scattering is proportional to density while bremsstrahlung is proportional to density squared. We have completed a survey of such events for 2011–2012, not yet published, and remark that the HMI team have now enlarged their field of view (January 2015) to enhance such future observations.

1.1.4.6 ***Temporal Evolution of Flare Emission***

The impulsive phase of a solar flare is characterized by impulsive hard X-ray emission thought to be linked to the fundamental physics of particle acceleration and flare energy release. It is now well known that similar impulsive signatures are also evident at other wavelengths

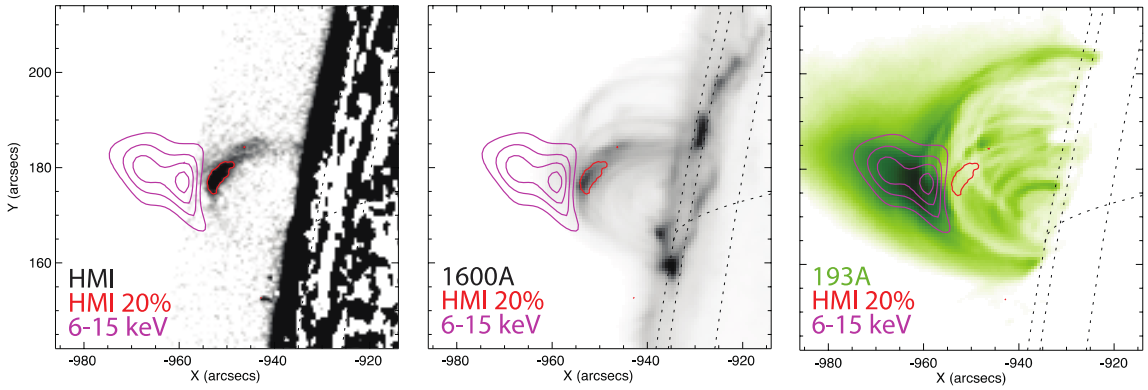

Figure 10. HMI/RHESSI/AIA observations of a post-flare loop system. HMI detects WL emission from a catastrophically cooled flare loop, while RHESSI sees hot loops at higher altitudes before they cool (from Martinez Oliveros et al. 2014).

associated with emission from thermal plasma. They can be revealed by taking the time derivative of the light curves, exploiting the Neupert effect in which the integral of the microwave or hard X-ray time history is often found to match the time profile in soft X-rays. Simões et al. (2014) have shown that these pulsations in the time derivative are evident in the GOES time profiles for all 35 X-class flares observed since September 2010, when GOES-15 became operational with its improved digitization and 2-s time resolution. In many cases, the so-called quasi-periodic pulsations (QPP) detected in the GOES time derivative plots closely match those seen in hard X-rays using RHESSI and/or Fermi/GBM data.

Recent work by various authors (e.g., Inglis & Dennis 2012, Inglis & Gilbert 2013) using RHESSI imaging capability shows that QPP are often associated with significant X-ray footpoint motions with velocities in the range ~50–100 km/s. Inglis & Gilbert (2013) combined RHESSI and SDO observations to perform a detailed correlation study between QPP temporal and spatial evolution and other observable flare phenomena. They demonstrated that QPP observations must be considered in the full 3D context of flares and that the linking process between the observed pulsations and footpoint motions must lie in the coronal sites of magnetic reconnection or particle acceleration.

1.1.5 Science Goal 5 – Global Structure of the Photosphere

Progress in this field has been slow because of the difficulty in analyzing the massive amounts of data on the optical solar disk from RHESSI's aspect system, and the need to correctly account for all possible systematic effects. The new work has concentrated on determining the pole-to-equator temperature gradient with perhaps an order of magnitude greater accuracy than has previously been possible.

Because of its requirement for sub-arcsecond aspect information, RHESSI incorporates correspondingly precise tools for image reconstruction and alignment, including the solar aspect system (SAS, described in Section 2.2.3). These requirements resulted in a major significant additional capability for RHESSI to study the Sun at visible wavelengths with a rapidly rotating telescope in space, a method never previously employed. The SAS consists of three 4-cm diameter plano-convex lenses that focus solar images in the continuum at 670 nm onto three linear CCDs 1.5 m away. The measured limb profiles (six in all, typically at a rate of 16 sets per second) provide the instantaneous pointing direction of the RHESSI instrument with sub-arcsecond accuracy. The rapid rotation of RHESSI (~15 rpm) around the solar direction provides another crucial advantage, since it allows for deconvolution of instrumental image distortion and greatly simplifies flat-field corrections, temperature corrections, and other factors that make photometry and astrometry difficult at the parts-per-million level.

Fivian et al. (2008) used these capabilities to obtain the most precise measurement of the solar oblateness, defined as the excess of the equatorial radius over the polar radius. Using only three months of the available data at an intermediate state of solar activity and screening against contamination by magnetic features at the limb, they reported a solar oblateness value

of (8.01 ± 0.14) milli-arcseconds. This is consistent with the Dicke estimate of 7.98 milli-arcseconds expected from the rotation of the Sun taken as being constant in cylinders around the rotational axis. It exceeds in precision all other measurements (both space and ground), including the more recent ones from SDO (Kuhn et al. 2012) and PICARD (Irbah et al. 2014).

Further work with these data has defined the pole-to-equator temperature gradient (Fivian and Hudson, 2013; Fivian et al. 2015). These temperature differentials are inferred from global brightness variations near the limb as seen by RHESSI using a screening against contamination by magnetic features, similar to the one described above. When all the data are used, the signal of the polar temperature excess appears to be compensated by the signal from magnetic elements at the active bands near the equator. Our best value of pole-to-equator temperature difference of ~0.05 K is taken when only 20% of the data are used. This is an order of magnitude smaller than previously reported (see Rast et al. 2008).

1.1.6 Science Goal 6 – Nonsolar Objectives

1.1.6.1 *Terrestrial Gamma-Ray Flashes (TGFs)*

TGFs, millisecond pulses of gamma radiation from lightning, have become a very active field of research worldwide, thanks in large part to RHESSI observations over the past decade. Progress over the last two years has resulted from discoveries about the extremes of TGF behavior and from the application of a new technique to detect weaker and shorter events in both RHESSI and Fermi/GBM data (Gjesteland et al. 2012).

Studies of the largest TGFs show that there are at least 40 events in which the TGF is so bright that RHESSI's pileup rejection circuit rejects all counts at the peak of the TGF (Kelley et al. 2015). These TGFs are estimated to produce about 10^{19} total gamma rays, or about a factor of 100 brighter than what has conventionally been considered a typical TGF.

Another new technique is being applied to RHESSI data in order to search for TGFs on the other end of the luminosity distribution – those too faint to be recognized individually (Smith et al. 2014b). RHESSI gamma-ray lightcurves at millisecond time resolution have been extracted in intervals surrounding over a million lightning flashes taking place below the spacecraft. The lightning is detected by the World Wide Lightning Location Network (WWLLN) in the VLF radio band. The average gamma-ray signal of a lightning stroke is determined from stacking the lightcurves when lightning is <700 km from the spacecraft. This average gamma-ray signal is surprisingly small, suggesting that there may not be many TGFs much fainter than the ones we observe.

Finally, a recent expansion of the trigger algorithm for RHESSI TGFs has revealed at least one significant difference between "normal" and "short" TGFs. The former last for several hundred microseconds to over a millisecond, and dominated the original RHESSI TGF catalog. The latter may be just as numerous, but were revealed in great numbers only in later analysis of RHESSI and Fermi/GBM data. Mapping the normal and short TGFs reveals that the latter are relatively (but not absolutely) more common over oceans than over land (Smith et al. 2014a). The meteorological/physical reason for this is not yet known.

1.1.6.2 *Cosmic Gamma-Ray Bursts (GRBs)*

Thanks to its broad energy range and wide field of view (>2π sr), RHESSI has made valuable contributions to the study of cosmic gamma-ray bursts (GRBs). These energetic transients have peak energies ranging from tens to hundreds of keV, and RHESSI continues to be a useful tool for continuum spectroscopy of GRBs (e.g., Bellm 2010; Ripa et al. 2012). RHESSI is also assisting with the prompt localization of GRBs (136 to date, K. Hurley, private communication) as part of the Interplanetary Network (IPN), which localizes GRBs by triangulation, comparing the time profiles seen by spacecraft in different parts of the solar

system. Prompt localization permits rapid follow-up by telescopes at all wavelengths from radio to X-rays, providing data on both the source of the explosion and the environment in the host galaxy.

RHESSI has also observed about seventy magnetar bursts, including the notable 2004 event from SGR 1806-20. A recent study (Huppenkothen et al. 2014) made use of RHESSI's high time resolution to argue for the presence of magnetic coupling between the crust and the core of the magnetar.

1.2 How the Prioritized Science Goals will be achieved

RHESSI remains a key complement to the HSO, uniquely providing information on the hottest plasma and the energetically important electrons and ions. **No other instrument can provide the location and spectra of the highest temperature plasma and the flare-accelerated electrons and ions.** Thus, the primary requirement for achieving our Prioritized Science Goals (PSGs) is for RHESSI to continue to provide X-ray and gamma-ray imaging spectroscopy during the declining phase of the current solar cycle.

In addition to the existing HSO space assets, eagerly anticipated new radio capabilities are expected to be available during this same time period, providing invaluable imaging spectroscopy observations over wide frequency ranges. These include several new major facilities including EVLA, ALMA, and other new facilities, but **the main new strength lies in the solar-dedicated EOVSA. We have never before had simultaneous microwave and RHESSI hard X-ray imaging spectroscopy, and this is the key to many problems of flare and active region development.** These two spectral bands show aspects of the same phenomena with distinctly different physical processes. In the past, we have had hints of this capability from the fixed-frequency "slices" of the microwave spectrum, and with EOVSA we will now get the full and detailed spectrum of the radio emission at every point in the image, and at every moment in time. EOVSA comes online this year (2015), and we expect that the first few M-class events will produce breakthrough observations – for which the RHESSI hard X-rays are required to establish "ground truth."

Finally, we note a comparable qualitative breakthrough in ground-based observations of the lower atmosphere. Several observatories (e.g., the Dunn Solar Telescope) now have broad-band capability for imaging spectroscopy in the energetically crucial photosphere and chromosphere (e.g., IBIS). In space, IRIS has begun to provide SUMER-like observations of flares for the first time, and again RHESSI hard X-rays are required to establish "ground truth" for the energetics.

1.2.1 Science Goal 1 – Evolution of Solar Eruptive Events

The second peak of solar activity in Cycle 24, with a resurgence in 2013, offers us many opportunities to compare the key RHESSI high-energy observations with copious new resources. The new and more comprehensive data set will allow us, for example, to test the ubiquity of the various magnetic scenarios that have been proposed. The SDO/AIA instrument provides us with detailed insights into the earliest phase of CME initiation and its plasma environment (Section 1.2.1.4) through its high-cadence imaging over a broad range of temperatures. Combined with RHESSI's observations of the accelerated particles in the associated flares and SDO/HMI observations of the magnetic field configuration and changes, these studies will provide us with information on the initiation of the instabilities and magnetic reconnection driving eruptive events.

The occurrence of solar energetic particle events has a strong solar-cycle dependence, and we expect many outstanding events to occur in the next years. To the pioneering work on the relation between flares, CMEs, and SEPs, we can now add information from SDO, Fermi, and several new ground-based radio astronomy facilities. STEREO, together with Wind, ACE, and

DSCOVR, will provide *in situ* measurements of SEPs at widely separated solar longitudes. Additionally, SDO/AIA will provide the high time cadence observations that were missing for observations taken during the last solar maximum. By tracking the electrons, imaged at the Sun using RHESSI HXR imaging spectroscopy data, through the interplanetary medium using the Type III radio emission, to the *in situ* detection by Wind and STEREO, we can trace and study the magnetic connectivity from the Sun to the Earth.

1.2.1.1 *Energetics of Solar Eruptive Events*

The energy partition study of Emslie et al. (2012) was restricted to 38 large SEEs, for which the dynamic range was comparable to the order-of-magnitude observational scatter, so that no clear variation in the partition of energy with flare size could be determined. A greater range of event sizes is needed to study the variation of these ratios, and thus to determine how the partitioning of the released energy does (or does not) vary with the overall energy in the event. Computations of the energies of the various energetically important components are being extended to 400 flares and CMEs observed with SDO, STEREO, and RHESSI. The different components include the thermal energy in soft X-ray and EUV emitting flare plasmas (Aschwanden et al. 2015), the nonthermal energy in accelerated particles, the kinetic energy of CMEs, the bolometric energies, and the radiated energies in soft X-rays and EUV. Statistics on these various energies will help guide us to the underlying physics.

1.2.1.2 *Quiescent eruptions and confined events*

RHESSI unexpectedly detected emission from a quiet-Sun filament eruption (Holman & Foord 2015). This expands the dynamic range of events that we can study so new observations of these eruptions will be sought. Tens of events have been identified in existing data sets, and future observations are planned that include coordinated studies with ground-based and space observatories.

We also expect to make progress by studying the so-called “confined events” that do not have associated CMEs. Thalmann et al. (2015) found that all of the 6 recent CME-less X-class flares from October 2014 show very slow ribbon motion and very steep RHESSI HXR spectra compared to typical eruptive flares, suggesting that a large fraction of the energy goes into the acceleration of low-energy electrons in these events. Hence, the released energy in CME-less flares still appears directly in the non-thermal electrons, but not at such high energies. This observational difference between these two types of events is currently unexplained but should contain a clue to the mechanism of eruption.

1.2.1.3 *HXR emissions from CMEs*

There is evidence that essentially all CME events should have extended HXR sources in the high corona Krucker et al. (2007, 2008), but these relatively faint emissions are very difficult to observe without complete occultation of the much brighter footpoint sources. The existing RHESSI database contains about 30 events of this type. The new complementary information provided by Fermi, and the new radio facilities such as EOVSA, LOFAR, MWA, and EVLA, will allow us to follow up on these discoveries with more explicit identification with specific acceleration mechanisms. These new radio telescopes will allow us, for the first time, to systematically image the different types of radio bursts to identify the different locations of electron acceleration in the lower corona during SEEs.

1.2.1.4 *IRIS observations: measuring flows within the SEEs*

With the availability of IRIS observations, we have a new diagnostic opportunity to study plasma motion within SEEs. Tian et al. (2014) reported IRIS observations in combination with imaging observations at other wavelengths that showed both up-flowing hot plasma and down-flowing cooler plasma at flare ribbons, as well as intriguing downflows towards the flare loop top

(Figure 11). A prime task for the next two years will be to study the time evolution in space of the flows in future events relative to the particle acceleration as derived by RHESSI. Additionally, the inclusion of NLFF magnetic field modeling will bring insights into where the magnetic energy is released.

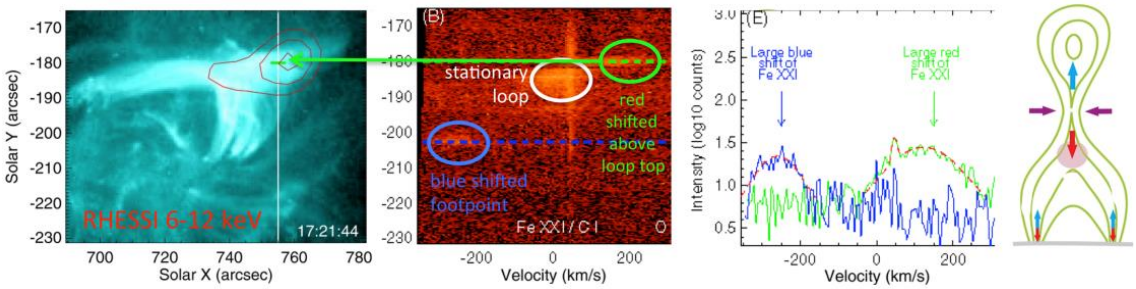

Figure 11. Combined RHESSI/SDO/IRIS observations of the C1.6 eruptive event SOL2014-04-19 (adapted from Tian et al. 2014). The RHESSI and SDO images (left) show the flare arcade with the RHESSI contours in red outlining the hottest plasma. The white vertical line gives the IRIS slit position. IRIS spectral data of the hot Fe XXI (10 MK) taken a few minutes before the RHESSI image are shown in the middle panel. While the thermal flare loop is stationary, there are down flows from the above the flare loop top (shown by green circle and by the green velocity profile). This is in agreement with the standard flare cartoon (right).

1.2.2 Science Goal 2 – Flare-accelerated Electrons

1.2.2.1 *Revising the classic thick-target beam model*

The observations discussed above point to the need for a substantial revision of the classic thick-target beam model. We have identified multiple lines of evidence that require major energy release at depths beyond the range of electrons accelerated in the corona, and yet a fully 3D congruence of the HXR source and the energy-release site now exists. How do we explain this? The advent of new resources (specifically IRIS and ground-based instruments such as IBIS and ALMA, which can now study the lower solar atmosphere with great diagnostic power) make a new departure possible.

1.2.2.2 *Occulted flares: directly observing coronal acceleration*

Despite the paradigm changes described above, we know that electron acceleration does take place in the corona, and that electron beams do form there. Occulted flare studies are a powerful tool to observe this relatively faint coronal emission that are otherwise lost because of the usually bright footpoints and the limited dynamic range of RHESSI images. About 10% of all flares are usefully limb-occulted so that the footpoints are obscured from view allowing RHESSI to study the coronal source(s) in isolation. In past studies, the magnetic configuration of such near-limb events could not be determined, but now STEREO can systematically provide information about the magnetic structure when the flare is not occulted as seen from at least one of the two spacecraft (e.g., Krucker et al. 2015). In addition, EUV ribbons imaged with STEREO show the likely location of the occulted HXR footpoints, and the CME geometry seen with the STEREO coronagraphs can be compared with the HXR coronal source location(s). A statistical study including all occulted RHESSI flares is underway. It will provide the best candidates of above-the-loop-top sources and potentially reveal flares where all but the above-the-loop-top source is occulted. This will allow us then to study the spectrum of the acceleration region in isolation. Such events would give an answer on the spectral shape at low energies and test the hypothesis that the acceleration mechanism produces electron spectra in the form of the Kappa function (e.g., Oka et al. 2015).

1.2.2.3 ***Complementary radio observations: EOVSA, EVLA, ALMA***

During the past 13 years of RHESSI observations, complementary radio observations were limited. Several new radio observatories have become operational in the last year or are coming online in 2015 providing powerful new broadband coverage of flare-accelerated electrons. Of greatest interest will be the newly operational EOVSA telescopes that will provide imaging-spectroscopy microwave observations. While tracking the electrons, such data also give quantitative measurements of the magnetic field strength. EOVSA is now partially observing in the frequency range from 2.5 to 18 GHz with spectral observations being already available as shown in Figure 12. Left: Time profiles at 11.4 GHz from EOVSA and 59 keV from RHESSI. Flare-accelerated electrons produce both types of emission (gyro-synchrotron in radio and bremsstrahlung in HXR) resulting in very closely matched time profiles. Right: EOVSA spectra at three different times during the impulsive phase of the flare as indicated by the arrows in the left-hand time profile plot.. The first imaging capability (i.e., getting centroid positions) is expected to be available by April 2015 and the first 2D images will be recorded later in the year.

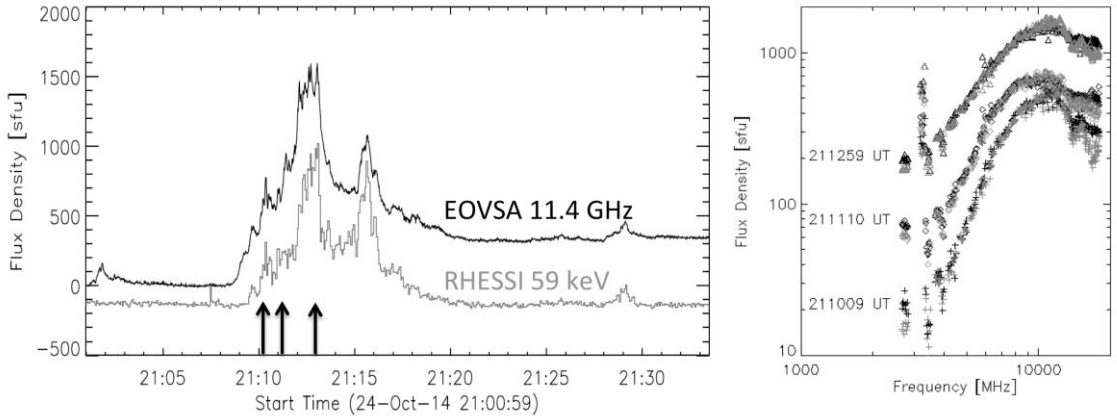

Figure 12. Left: Time profiles at 11.4 GHz from EOVSA and 59 keV from RHESSI. Flare-accelerated electrons produce both types of emission (gyro-synchrotron in radio and bremsstrahlung in HXR) resulting in very closely matched time profiles. Right: EOVSA spectra at three different times during the impulsive phase of the flare as indicated by the arrows in the left-hand time profile plot.

A major requirement for determining the energy budget in SEEs is information on the low-energy cutoff of accelerated electron distributions. Despite the obvious temporal correlation between radio-derived and HXR-derived electron fluxes, there is often a discrepancy between the spectral indices derived from the two observation sets (e.g., Holman 2003; White et al. 2011).

For coherent radio bursts that usually occur at lower frequencies than those currently covered by EOVSA, EVLA provides by far the best observations. However, its observation times for solar studies are very rare. The past observation runs have been successful in recording a few minor flares, but not yet a two ribbon flare or a large impulsive flare with a prominent type III radio burst. In the next two years, we expect at least a few EVLA solar flare observation runs to give us a chance to increase our database significantly.

Finally, we note the achievement of solar test observations of the powerful ALMA radio facility and its formal opening to solar proposals in the next opportunity cycle, expected later in 2015. This facility has now demonstrated excellent single-dish and interferometric capabilities with arcsecond resolution, high signal-to-noise ratio and radiometric precision in scanning mode, and high spectral resolution over a broad range of frequencies from 84 to 950 GHz. It will provide comprehensive new views of solar flares, in particular in the lower atmosphere that now seems to be decisively important. Figure 13 shows an image and a lightcurve from a single-

dish observation at 100 GHz of a small solar flare (SOL2014-12-14T19:52, C4.7) observed during the test observations in December 2014.

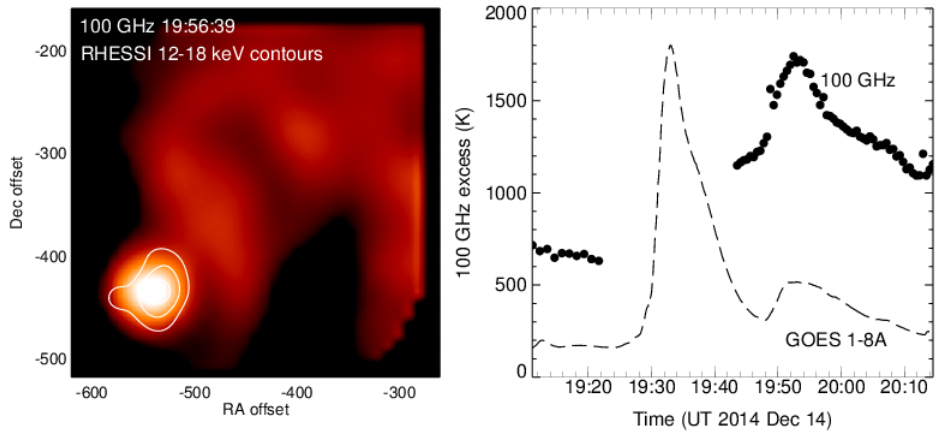

Figure 13. Left: ALMA image at 100 GHz constructed by fast scanning of a pencil beam with FWHM about one arc min. Right: the time series of the flare observation. Note the high SNR of the timeseries (preliminary and unpublished data, courtesy of Stephen White).

1.2.3 Science Goal 3 – Flare-accelerated Ions

The advent of Fermi observations of LDGRF ("sustained") gamma-ray emission at very high energies (e.g., Ajello et al. 2014) complements RHESSI's capabilities and offers a major challenge for identification and interpretation. We will continue the analysis of joint RHESSI/Fermi observations, with the potential for new events that exhibit both impulsive ion acceleration and long-duration >100 MeV emission. In past solar cycles, the declining phase has often been the time when large events tend to occur, such as the series of X-class flares in late 2006. RHESSI covers the same energy range as GBM, but with significantly better spectral resolution, which allows for a better determination of the ion spectrum at tens of MeV. RHESSI imaging studies of X-rays and ion-associated lines can be compared with the centroid locations as accurate as ~30 arcsec determined by Fermi/LAT for the >~100 MeV LDGRFs. Visibility-based analysis of RHESSI observations, already used for imaging different temperature components in the X-ray range, will be applied in the gamma-ray range to separate the line emission from the underlying bremsstrahlung continuum.

RHESSI gamma-ray observations during the declining phase of Cycle 24 are dependent on the operational state of the spectrometer (discussed in Section 2.2.1) and the level of solar activity. After each periodic anneal, radiation damage broadens the spectral resolution of the rear detector segments and reduces their effective sensitive volume. For about a year after each anneal, the rear segments are still able to achieve spectral resolutions of less than a few tens of keV in the MeV range, still significantly better than the Fermi GBM BGO detectors. For two or three years after an anneal, before the level of radiation damage becomes severe, the FWHM spectral resolution of the front segments is a few keV up to a maximum energy of >2.3 MeV, so that it is possible to use the front segments to detect and study intrinsically narrow lines such as the annihilation and the neutron capture lines. In comparison to the rear segments, the front segments have smaller photo-peak efficiencies (~50% at 511 keV and ~15% at 2.2 MeV) and greater deadtime at the most intense peaks of flares, but they also have lower background, so comparable science up to 2.3 MeV can still be achieved. Even with unsegmented detectors, RHESSI will be sensitive to gamma-rays and to the neutron-capture line in large flares but with degraded energy resolution.

1.2.4 Science Goal 4 – Flare-heated Plasma

1.2.4.1 *Flare ribbons: energy input and response*

In the next two years we expect to complete a major revision of the standard thick-target beam model (see also Science Goal 2). For this task we have a substantial advance in the availability of a large number of complementary data sets provided by IRIS, SDO, HINODE, STEREO, and ground based optical and radio observatories such as EOVSA and ALMA. RHESSI data are playing a key role in these studies, as it is the only instrument that provides the energy spectrum and location of the non-thermal electrons. All other instruments observe only the thermal and flow responses to the energy deposition.

The newly observed events during the next years will significantly increase our flare list; in particular for joint IRIS observations. The initial RHESSI/IRIS results presented in the previous section show the great potential, but it is also clear that we are just at the beginning of understanding how to fully exploit these data sets. Additionally, the newly available de-saturation algorithm to reconstruct saturated AIA images (Schwartz et al. 2014) will provide the required input to properly see the EUV counterparts of the HXR footpoints (Figure 14) and to compute the DEM of the flare ribbons. Combining the RHESSI/IRIS results with DEM analysis from SDO and HINODE (e.g., Graham et al. 2013), we will have by far the most complete set of data ever to do detailed comparisons with simulations.

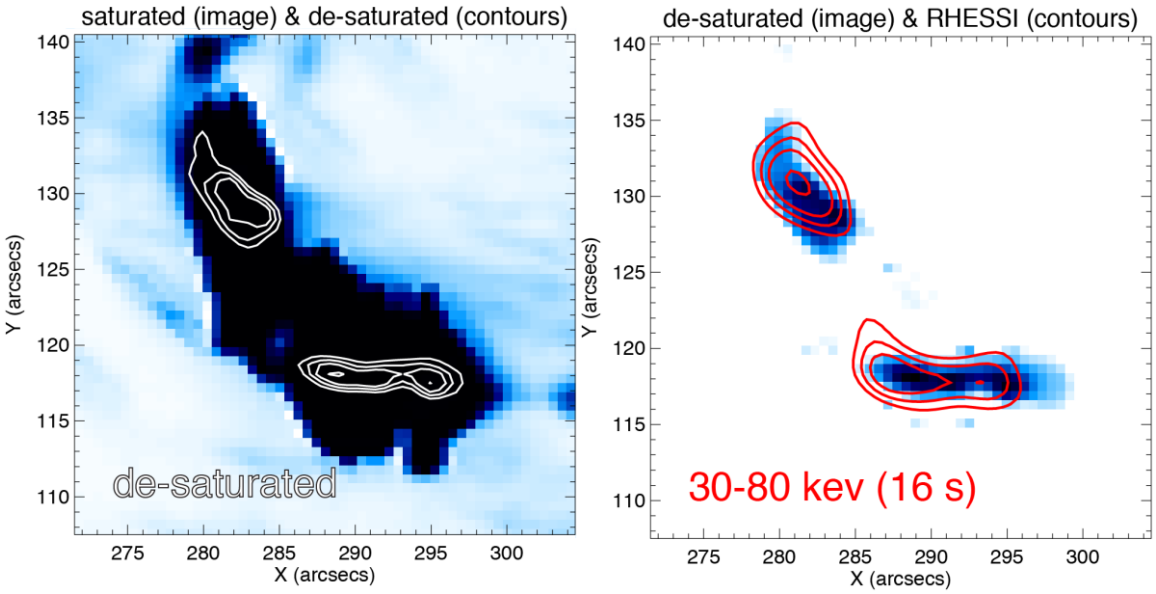

Figure 14. Example of an AIA image at 2011 Sep 6, 22:18:38UT, showing flare ribbons de-saturated using the algorithm described in Schwartz et al. (2014). Left: saturated AIA 131 image of the flare ribbon with white contours showing the de-saturated image. Right: de-saturated image with RHESSI 30–80 keV sources shown by the red contours.

1.2.4.2 *HXR and WL flare studies*

We have already started a statistical study of all large flares jointly observed by RHESSI and SDO/HMI or Hinode/SOT. We have more than 4 years of observations with about 60 large flares (typically GOES class M5 and larger) that show clear emission at both wavelengths, and we expect more than 100 flares by the end of the solar cycle. The size and quality of the statistical sample will be unique and will provide a definite answer to the question of whether all flares have WL emissions or if there is a subclass without a HXR counterpart. The study will provide quantitative measurements that will be used as input to the simulations.

Co-spatial HXR and WL sources have major implications for the heating of flare ribbons by flare-accelerated electrons (Krucker et al. 2015). As the WL sources are indicative of temperatures of ~10^4 K (i.e., low compared to coronal temperatures of several MK), flare-accelerated electrons are only heating the flare ribbons to these temperatures. This suggests that flare-accelerated electrons may not drive chromospheric evaporation directly, since the energy appears as UV/optical/IR radiation. Nevertheless, the poorly observed low-energy end of the flare accelerated electron distribution at higher altitudes can still heat footpoint plasma to coronal temperatures and drive evaporation. To have enough energy, flare-accelerated electrons need to extend down to low energies of the order of ~10 keV. However, non-thermal HXR emission from such energies are generally difficult to observe given the much brighter thermal emission at the same energies. The best chance of detecting such low-energy non-thermal emission is in so-called early impulsive flares (e.g., Sui et al. 2007), where the non-thermal emission is very prominent right at the onset of the increase of the thermal emission.

1.2.5 Science Goal 5 – Global Structure of the Photosphere

The RHESSI optical aspect system continues to produce valuable science that is outside the primary goals of RHESSI: the characterization of the shape and brightness of the solar photosphere at the highest levels of precision (see Sections 1.1.5). To further this effort, we will continue to operate in campaign mode to obtain much larger data bandwidths during special conditions, such as RHESSI anneal operations or SDO roll maneuvers performed twice yearly when SDO gets comparable global imaging information.

This application becomes all the more important as the mission life increases because these precise measurements can be applied to solar-cycle variations. The solar oblateness and the limb-darkening function, as well as any large-scale structures in photospheric brightness, may vary systematically with the solar cycle. RHESSI SAS observations now contain over 4×10^{10} data points at the limb. This database is unique in several ways and represents a major contribution by RHESSI to our knowledge of solar global structure and variability, the underpinning of the solar dynamo action and all that we study. We believe that this capability should be extended as long as possible, and eventually replaced with a similar overlapping capability for future observations.

1.2.6 Science Goal 6 – Nonsolar Objectives

Extending RHESSI TGF observations into the future provides more benefit per year of data than just the extension of the existing database. Because atmospheric electricity is a rapidly changing and expanding field, each year there is a wider variety of contextual data available, and in this era of TGF studies, it is the quality and amount of contextual data on lightning characteristics that drives most of the new science. Similarly, there are more observations than ever per year of sprites, elves, gigantic jets, and other exotic "transient luminous events", all of which might prove to have high-energy emission of their own if a sufficiently bright and well-timed event is found. RHESSI has a higher-latitude orbit than the other currently operating major missions doing TGF science (Fermi and AGILE), and can sample storms in non-tropical regions, providing a greater variety of meteorological context and therefore a better sense of the role of TGFs in different storm types.

RHESSI TGF studies have traditionally been done using only the rear segments, but they are actually quite insensitive to the de-segmentation of some detectors and loss of energy resolution. This is because TGFs have smooth continuum spectra, far harder than any solar or astrophysical source. Hence, the threshold to trigger a TGF can be set at a higher energy than that of most solar photons with little loss of sensitivity.

1.3 Potential for Performance from FY-16 through FY-20

1.3.1 Relevance to the SMD Science Plan and contributions to HSO

RHESSI is directly relevant to achieving NASA's strategic goal for Heliophysics to "Understand the Sun and its interactions with the Earth and the solar system." It addresses the SMD Science Question – "What causes the Sun to vary?" and the following Science Area Objectives: "Understand the fundamental physical processes of the space environment from the Sun to Earth" and "Maximize the safety and productivity of human and robotic explorers by developing the capability to predict the extreme and dynamic conditions in space."

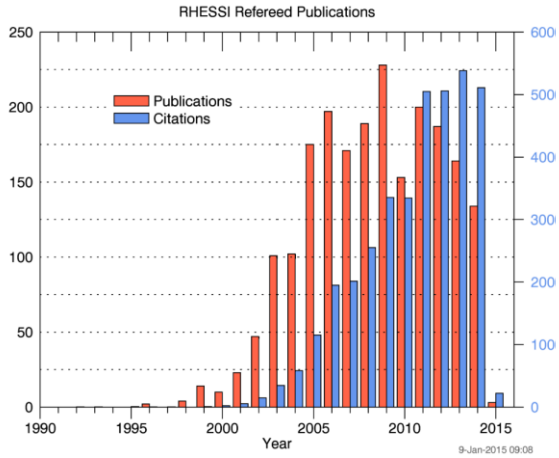

Figure 15. Number of refereed publications (red, left scale) per year that involve RHESSI and the number of citations per year to those papers (blue, right scale)

1.3.2 Productivity and Vitality of Science Team

The first thirteen years of RHESSI operations have been extraordinarily productive. To date, RHESSI observations have contributed to ~2,000 refereed papers and over 100 PhD and master's theses listed at the following web site: http://hesperia.gsfc.nasa.gov/rhessi3/news-and-resources/results/. The annual numbers of refereed articles and citations related to RHESSI are shown in Figure 15 as obtained from the NASA ADS web site by searching for the words "HESSI" or "RHESSI" in the title, abstract, or text.

The current status of our understanding of solar flares recently appeared in a complete ~500-page volume of *Space Science Reviews* (Volume 159, 2011) entitled "High-Energy Aspects of Solar Flares." The nine individual chapters are available at http://hesperia.gsfc.nasa.gov/rhessi3/news-and-resources/results/monograph.html.

The RHESSI PI team created and supports the Max Millennium program accessible at http://solar.physics.montana.edu/max_millennium/. It serves several functions that are key to the successful acquisition of observationally complete datasets and the full scientific exploitation of those observations. These functions include the daily recommendations of targets for joint observations and the establishment of joint observing plans with specific scientific goals in the event of predicted major flare activity.

RHESSI personnel have initiated, organized, and attended many scientific meetings and special sessions, including thirteen RHESSI-specific workshops with a fourteenth planned in August 2015 at NJIT in Newark, NJ. (http://ovsa.njit.edu/rhessi14/). Several international teams of scientists have also met under the sponsorship of the International Space Science Institute (ISSI) to explore issues related to RHESSI science. We will continue this sequence of scientific meetings.

Beginning in March 2005, the RHESSI team began a biweekly series of "Science Nuggets" at http://sprg.ssl.berkeley.edu/~tohban/wiki/index.php/RHESSI_Science_Nuggets. Each Nugget is a brief report that is intended to introduce various aspects of the scientific material to a technically competent audience, and often include novel as-yet-unpublished insights. Both RHESSI team members and a worldwide community of interested scientists contribute to the Nuggets, now approaching 250 in number.

1.3.3 Data Accessibility and Usability

Full details of RHESSI data accessibility and usability are given in the accompanying Mission Archive Plan. The data archive contains the full Level-0 telemetry data, the RHESSI flare list, and quicklook lightcurves, spectra, images, and housekeeping plots for the entire mission. These plots, as well as context information discussed below, are easily accessed using the RHESSI Browser, http://sprg.ssl.berkeley.edu/~tohban/browser/. The archive, currently ~9 TB, resides on a private server at SSL and two public servers, one at Goddard and the other at FHNW in Switzerland. Extensive RHESSI documentation is at http://hesperia.gsfc.nasa.gov/rhessi/, with comprehensive descriptions of the mission, the instrument, the science objectives, data analysis techniques, the software, and the data archive. In addition, support personnel are available at all three data sites to guide scientists in using the software and interpreting the results.

1.3.3.1 *Software*

One of the unique characteristics of RHESSI is that the telemetered data contain detailed information on each detected photon. This provides the flexibility to make *ex post facto* decisions and tradeoffs associated with time resolution, energy resolution, imaging resolution and field of view, enabling the analyst to optimize these parameters as needed. Another advantage of this photon-oriented database is that ongoing improvements to the software and instrument calibration can be fully applied retroactively to all the data since the beginning of the mission.

The complete RHESSI software package necessary for the analysis of all RHESSI data is available online as part of the Solar Software (SSW) tree. The software generates image cubes (in time and energy), spectra (either spatially-integrated or feature-specific), and light curves, and provides support for comparisons with data products from other missions.

Spectral analysis capabilities are now enhanced by adding templates for the gamma-ray lines between ~300 keV and 10 MeV that depend on the spectrum, composition, and directionality of the accelerated ions, and the ambient solar abundance. Templates of pion-decay gamma-ray spectra extending to higher energies covered by Fermi GBM and LAT are also available.

Powerful visibility-based X-ray analysis can now be routinely carried out using several different image-reconstruction algorithms that include the capability to compute spectrally regularized image cubes. Visibilities are calibrated, instrument-independent, Fourier components of the source image. Mathematically, they correspond to the output of a single baseline of a radio interferometer. For RHESSI, they represent an intermediate data product directly obtained from the observed time-modulated light curves. The basic visibility software has enabled the accurate determination of HXR source sizes (useful for example to convert thermal emission measurements to electron densities), and the evaluation of albedo; it was the computational tool of choice in obtaining several of the recent results discussed above. The ESA-funded project, High Energy Solar Physics in Europe (HESPE http://www.hespe.eu/), has compiled a set of visibility-based data spanning the duration of the RHESSI mission, thus allowing the essential imaging spectroscopy information to be encoded very compactly.

1.3.3.2 *Facilities for Multi-wavelength Analysis*

The following steps have been taken to support the convenient integration of RHESSI data into studies involving other wavelength regimes:

- The RHESSI software package includes flexible tools for accessing and integrating multiple data sets (e.g. overlaying images from different instruments). Coalignment is simplified

since the absolute positions of RHESSI images are inherently determined to arcsecond accuracy.

- The Synoptic Data Archive at the GSFC Solar Data Analysis Center (SDAC) provides access to image, spectral, and lightcurve datasets spanning a broad wavelength range from radio to gamma-rays. .
- SDO/AIA cutout image FITS files and movies generated for every RHESSI flare after September 2010 are linked from the RHESSI Browser, and the FITS files are available through the Synoptic Data Archive mentioned above.
- Science-ready RHESSI time profiles, images, and spectra conforming to SPASE guidelines are now being generated for each event. They will be accessible from the RHESSI Browser, through the VSO (and therefore the Synoptic Archive), and in (J)Helioviewer.
- The spectral analysis software package written for RHESSI also handles X-ray and gamma-ray data from Fermi/GBM and LAT, MESSENGER/SAX, and SOXS, allowing users to analyze these different data types alone or jointly with RHESSI data in a familiar environment

  The RHESSI web-based Browser is available at the following location:
  http://sprg.ssl.berkeley.edu/~tohban/browser/?show=grth+qlpcr

It provides a quick and easy way to display the wealth of RHESSI quicklook plots and to investigate the context of RHESSI events with data from many other instruments.

1.3.4 Promise of future impact and productivity

RHESSI is still fully operational and is expected to continue in this state for at least another two years. It continues to be the only mission capable of solar HXR imaging spectroscopy and is likely to retain that unique position until the launch of the Spectrometer Telescope for Imaging X-rays (STIX) on the European Solar Orbiter with a nominal start of science observations in 2020. Thus, it is critical that RHESSI be available for as long as possible to provide the high-energy coverage of the flares seen with the advanced instrumentation on IRIS, SDO, Hinode, STEREO, and Fermi, and the improved ground-based radio and optical observatories such as EOVSA and EVLA.

The long-term prospects for the RHESSI germanium detector performance are discussed in Section 2.2.1. In summary, we expect that operations can continue well into 2017, with a possible fifth anneal sometime in 2016, with some reduction in performance but with the core HXR imaging spectroscopy capability retained.

2 TECHNICAL AND BUDGET

2.1 Spacecraft

RHESSI was launched on February 5, 2002, into a circular orbit with an altitude of 600 km and an inclination of 38°. The observatory continues to function very well after 13 years of operations in its present 517 x 510 km orbit. All of its subsystems are fully operational. RHESSI has no expendables and the relatively low level of solar activity means that its orbital decay has been less than predicted. The latest orbital lifetime predictions made by Flight Dynamics Support Services (Code 595) at Goddard show that the “Mean Nominal” predicted reentry date is March 2022 and the “Early +2 Sigma” date is September 2021.

The solar array power output has declined slightly since launch but the battery voltage and absolute and differential pressures have been relatively stable for the past 3 years. The average spacecraft temperature has increased by only ~1° C since launch. The S-band transceiver still generates a stable output power of 5 W with clean BPSK modulation at 4.0 Mbps, and the receiver shows no signs of deterioration in performance. The attitude control system is stable and the C&DH subsystem shows no signs of degradation.

The telecommunications subsystem has generally been stable since launch. However, following the detector annealing in November 2007, the receiver is seeing increased noise from the spacecraft power bus, and ATS table loads are unsuccessful during nighttime passes. This situation is easily mitigated by scheduling daylight passes at the Santiago ground station during infrequent periods when both the Berkeley and Wallops ground stations have only nighttime passes.

In 2010, following a power-related anomaly with the spacecraft on March 16 of that year, all over-current and under-voltage hardware trip circuits, as well as the over-current and battery under-pressure protection in the flight software, were disabled. This decision was made with concurrence of the Space Science Mission Operations (SSMO) Project at NASA/GSFC and the Systems Engineer at Orbital Science Corporation. The risk associated with disabling the on-board fault detection and correction system was assessed to be lower than the risk of losing the cryocooler or the germanium detectors in case of a recurrence of the anomaly.

Aside from the described problems, all other subsystems and sensors are functioning nominally. Overall, there is no reason to believe that the spacecraft will not continue to function very well over the next several years.

2.2 Instruments

2.2.1 Spectrometer and Cryocooler

The RHESSI germanium spectrometer and its Sunpower cryocooler continue to perform well. The cryocooler has operated nearly continuously for more than 130,000 hours. While showing signs of reduced cooling power, it is continuing to operate with an input power of 67 watts and negligible vibration. The detector temperature has increased from 74 K to ~130 K over the course of the mission, but spectral performance has not been affected by any associated increase in thermal leakage current. The only guideline that we have for the high-temperature behavior of the RHESSI detectors comes from studies of non-RHESSI germanium detectors (Pehl et al. 1973), some of which have been observed to reach a problematic level of leakage current at ~150 K. It is unclear whether this temperature limit applies to our detectors, but we do not anticipate reaching this temperature regime until 2017.

RHESSI's germanium detectors are each in the shape of a cylinder with a small central bore that runs from the bottom up to about 1 cm from the top. Although each detector consists of a single crystal of pure germanium, it is divided electrically into two segments. The front ~1.5-cm thick segment is read out through one electrical contact at the top of the inner bore and the rear ~7 cm through another contact further down the bore. This is accomplished by lining the bore with a conductive contact of diffused lithium ions that is interrupted about 1 cm from the top end of the bore. The front segment stops most hard X-rays below ~200 keV, and is used for X-ray science down to ~3 keV, while the rear segment registers gamma rays above ~100 keV, in particular in the nuclear line region. The vast majority of flares observed by RHESSI are studied primarily using front-segment data; only a small fraction of M-class flares and about half of all X-class flares produce gamma-ray emission that enables use of the rear segments.

Radiation damage from encounters with radiation belt protons in the South Atlantic Anomaly gradually degrades the energy resolution of RHESSI's detectors, and, when it advances to an extreme degree, renders the outer cylindrical layer of the detector volume insensitive to interactions. This has a bigger effect on the gamma-ray performance than on the X-ray performance. Four times over the course of the mission, in November 2007, April 2010, January 2012, and July 2014, RHESSI's germanium detectors were annealed to reverse the effects of radiation damage resulting in the recovery of the energy resolution and sensitive volume. In this procedure, the cold plate to which they are mounted is heated to ~100° C, causing the detectors to reach a similar temperature. While the mobility of the atoms in the

lattice is not sufficient to "heal" the disordered regions produced by proton and neutron interactions, it renders these disordered regions unable to trap moving holes in the crystal, and therefore neutralizes them in terms of their effect on detector performance.

Unfortunately, these periods of high temperature also cause the lithium ions that make up the inner contacts to drift deeper into the crystal, which can “short out” the separation between the front and rear segments. The resulting unsegmented detector has degraded performance compared to a normal front segment. It has higher background rates since that is now from both the front and rear detector volumes; it has broadened energy resolution of typically ~10 keV FWHM at 100 keV as opposed to 1–2 keV, and it has an elevated threshold energy of ~20 keV vs. 3 keV. Unsegmented detectors can, however, still be used for RHESSI’s core observational capability of imaging spectroscopy above ~20 keV with no loss in angular resolution or sensitivity to events well above background. This type of electrical shorting is actually counteracted by later accumulation of radiation damage, which causes the active volume to shift towards the inner contacts, allowing it to “see” the contact separation more easily. Following the 2012 anneal, two of the nine detectors lost segmentation, but both regained segmentation at a later time. Following the 2014 anneal, four detectors lost segmentation, but at the time of this writing, two of those four have since regained segmentation.

Based on the history of detector degradation following the previous anneals, we may perform a fifth anneal in ~2016 if cryocooler performance allows. If we choose to no longer anneal the detectors, gamma-ray performance will be significantly degraded, but X-ray spectral resolution will be better or comparable to unsegmented detectors for years, albeit with significant reductions in effective area and corresponding losses in sensitivity.

Even with unsegmented detectors or degraded detectors, RHESSI’s core science is achievable. Hard X-ray imaging above 20 keV is virtually unaffected except for weak flares where sensitivity above the increased background becomes an issue. Figure 16 shows images of a flare from 2012 July 19 made with subcollimators 1–5. At the time, the detectors for subcollimators 2 and 4 were unsegmented, and these are also the same detectors that are currently unsegmented. Aside from the changes in the apparent source sizes – each subcollimator measures a different angular scale – the images are all of comparable quality. Also, the best-fit power-law index (γ) has the same value within uncertainties for all detectors, independent of their segmentation status.

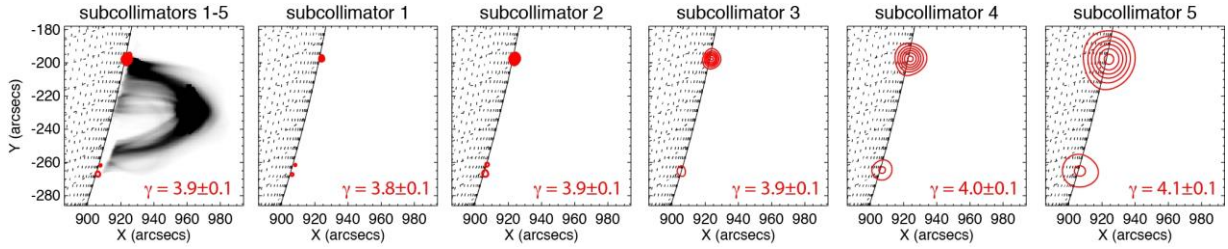

Figure 16. Imaging footpoints at 35–80 keV during a flare on 2012 July 19 with RHESSI's five finest grids. The image quality and the best fit power-law spectral index (γ) using the unsegmented detectors (#2 and #4) are unaffected. The background image in the first panel is from SDO/AIA at 131 Å.

This demonstrates that RHESSI will continue making what is probably its most important contribution in the mature phase of its mission: revealing the sites of high-energy electron interactions in flares that are studied across wavelengths by a variety of spacecraft and ground-based instruments. Imaging spectroscopy will still be possible in relatively broad energy bands above the ~20 keV threshold. For example, energy bins of 20–30 keV and 50–70 keV could still provide cleanly separated images of superhot thermal emission and nonthermal emission in a

large flare. Spatially integrated spectra will still be possible above ~20 keV so that RHESSI will still be able to provide estimates of the total energy in nonthermal electrons for input to flare models.

2.2.2 Imager

The RHESSI imager subsystem consists of nine rotating modulation collimators, each of which has a pair of widely separated grids. A metering structure maintains the relative twist alignment of the nine grid pairs. The imaging subsystem is inherently stable and has shown no evidence of change in grid alignment. Improved analysis techniques are refining the calibration of the grid parameters and locations (now known to submicron accuracy), the results of which are built into the software package and are applicable to all data acquired since launch.

2.2.3 Aspect System

There are three parts to the RHESSI aspect system. The absolute pitch and yaw angles relative to Sun center are provided by the Solar Aspect System (SAS), with sub-arcsecond accuracy. The roll angle is provided by two redundant side-looking star scanners, a CCD Roll Angle System (RAS) and a PhotoMultiplier-Tube Roll Angle System (PMT-RAS).

The SAS consists of a set of three identical lens/sensor subsystems, each of which focuses a narrow-bandwidth image of the solar disk onto a linear CCD array. No anomalies in its operation have been observed and the sensitivity is stable with an order of magnitude margin before there would be any compromise in accuracy. The PMT-RAS continues to provide the roll aspect knowledge upon which most of the solar imaging is based. Its response has remained stable since launch, easily meeting the 1 arcminute roll-angle requirement with a large margin in sensitivity. The CCD RAS has also proven to be stable and able to meet the same roll-angle requirement. Its data are used to fill occasional gaps in the PMT-RAS coverage.

2.3 Ground System

In 1999, a multi-mission operations facility was established at SSL to support the RHESSI and FAST missions. The joint facility, which now also supports other missions, includes the Mission Operations Center (MOC), the Science Operations Center (SOC), the Flight Dynamics Center (FDC), and the Berkeley Ground Station (BGS). Backup support is provided by Wallops Island (WGS), Santiago (AGO), and the DLR ground station at Weilheim, Germany. BGS has supported more than 25,000 RHESSI passes since launch - 5–6 passes per day on average. WGS and AGO support typically 4 passes per day combined. The average daily data volume is 1.8 GB with an overall telemetry recovery efficiency of ~99%.

RHESSI normal operations comprise mission planning functions, command load generation, real-time pass supports, spacecraft state-of-health monitoring, data trending, instrument configuration, and science data recovery and archiving. Generation of all ephemeris and mission planning products is based on two-line element sets that are downloaded from the Space-Track.org web site, quality checked and archived locally in a fully automated mode. Spacecraft ATS loads are built by the Flight Operations Team (FOT) and uploaded to the spacecraft multiple times per week. Every six weeks, the spacecraft is spun up from about 14.5 rpm to its nominal spin rate of 15 rpm.

The RHESSI Science Operations Center, located at SSL, consists of a RAID server, with ~13.7 TB of data capacity, and six processors. The SOC receives RHESSI data after every ground-station contact and automatically processes them to create Level-0 data files. As of January 2015 there are ~95,000 Level-0 files, containing 9 TB of data. Other automated procedures generate quick-look data containing the RHESSI observing summary, flare list, and quick-look light curves, images, and spectra.

2.4 References

Ackermann, M., et al. 2014, ApJ, 787, 15
Ajello, M., et al. 2014, ApJ, 789, 20
Alaoui, M., & Holman, G. D. 2015, in preparation
Allred, J. C., et al. 2005, ApJ, 630, 573
—. 2015, ApJ, to be submitted
Aschwanden, M. J., et al. 2014, ApJ, 797, 50
—. 2015, ApJ, submitted
Bain, H. M., & Fletcher, L. 2009, A&A, 508, 1443
Battaglia, M., & Benz, A. O. 2009, A&A, 499, L33
Battaglia, M., et al. 2015, in preparation
Bellm, E. C. 2010, ApJ, 714, 881
Bian, N. H., et al. 2014, 796, 142
Caspi, A., et al. 2014a, ApJ, 781, 43
—. 2014b, ApJ, 788, 31
—. 2015, in preparation
Chen, B., et al. 2013, ApJ, 763, L21
—. 2014, AGU abstract SH23A-4149
Chen, Q., & Petrosian, V. 2013, ApJ, 777, 33
Codispoti, A., et al. 2013, ApJ, 773, 121
Dennis, B. R., et al. 2015, ApJ, submitted
Dickson, E. C. M., & Kontar, E. P. 2013, Sol. Phys., 284, 405
Emslie, A. G., et al. 2012, ApJ, 759, 71
Fivian, M. D., et al. 2008, Sci., 322, 560
Fivian, M. D. and Hudson, H. S. 2013, AAS/SPD meeting, 44, #100.121
Fivian, M. D. et al. 2015, in preparation
Fleishman, G. D., & Kontar, 2010, ApJ, 709, L127
Fleishman, G. D., et al. 2013, ApJ, 768, 190
Gjesteland, T., et al. 2012, GRL, 39, L05102
Glesener, L., et al. 2013, ApJ, 779, 29
Graham, D. R., et al. 2013, ApJ, 767, 83
Gritsyk, P. A., & Somov, 2014, Astron. Lett., 40, 499
Hannah, I. G., et al. 2011, Space Sci. Rev., 159, 263
Heinzel, P., & Kleint, L. 2014, ApJ, 794, L23
Holman, G. D. 2003, ApJ, 586, 606
—. 2012, ApJ, 745, 52
Holman, G. D., & Foord, A. 2015, submitted
Huppenkothen, D., et al. 2014, ApJ, 793, 129
Hurford, G. J., et al. 2003, ApJ, 595, L77
—. 2006, ApJ, 644, L93
Inglis, A. R., & Christe, S. 2014, ApJ, 789, 116
Inglis, A. R., & Dennis, B. R. 2012, ApJ, 748, 139
Inglis, A. R., & Gilbert, H. R. 2013, ApJ, 777, 30
Irbah, A., et al. 2014, ApJ, 785, 89
Kaufmann, P., et al. 2013, ApJ, 768, 134
Kelley, N. A., et al. 2015, in preparation
Kleint, L., et al. 2015, in preparation
Krucker, S., & Battaglia, M. 2014, ApJ, 780, 107
Krucker, S., et al. 2007, ApJ, 669, L49
—. 2008, A&A Rev., 16, 155
—. 2013, A&A Rev., 21, 58
—. 2015, in preparation
Kuhn, J. R., et al. 2012, Sci., 337, 1638
Landi, E., et al. 2010, ApJ, 711, 75
Li, T. C., et al. 2014, ApJ, 793, L7
Liu, W., et al. 2013, ApJ, 767, L168
Martinez Oliveros, et al. 2012, ApJ, 753, L26
—. 2014, ApJ, 780, L28
Milligan, R. O., et al. 2014, ApJ 793, 70
Oka, M., et al. 2013, ApJ, 764, 6
—. 2015, ApJ, 799, 129
Pehl, R. H., et al. 1973, IEEE Trans. Nucl. Sci., 20, 494
Patsourakos, S., et al. 2013, ApJ, 764, 125
Rast, M. P., et al. 2008, ApJ, 673, 1209
Raulin, J.-P., et al. 2014, Sol. Phys., 289, 227
Reid, H., et al. 2014, A&A, 567, A85
Ripa, J., et al. 2012, ApJ, 756, 44
Ryan, D. F., et al. 2014, Sol. Phys., 289, 2547
Ryan, J. 2000, Space Sci. Rev., 93, 581
Saint-Hilaire, P., et al. 2014, ApJ, 786, L19
Schwartz, R. A., et al. 2014, ApJ, 793, L23
Simões, P. J. A., & Kontar, E. P. 2013, A&A, 551, A135
Simões, P. J. A., et al. 2014, arXiv,1412.3045
Smith, D. M., et al. 2014a, ICAE Conference abstract O-06-04
—. 2014b, AGU abstract AE33A-07
Su, Y., et al. 2013, Nature Phys. Sci., 9, 489
Sui, L., et al. 2007, ApJ, 670, 862
Sylwester, B., et al. 2014, ApJ, 787, 122
Testa, P., et al. 2014, Science, 346, 1255724
Thalmann, J. K., et al. 2015, ApJ, to be published
Tian, H., et al. 2014, 797, L14
Torre, G., et al. 2015, in preparation
Varady, M., et al. 2014, A&A, 563, A51
Vestrand, W. T. and Forrest, D. J. 1993, ApJ, 409, 69L
Warren, H. P. 2014, ApJ, 786, L2
White, S. M., et al. 2011, Space Sci. Rev., 159, 225
Xu, Y., et al. 2004, ApJ, 607, L131

APPENDIX
3 RHESSI MISSION ARCHIVE PLAN

3.1 Introduction

Normal RHESSI (Lin et al. 2002) operations are largely autonomous, with an almost daily command upload containing the telemetry schedule and occasional adjustments to instrument parameters. Except during detector anneals, eclipse periods, passages through the South Atlantic Anomaly, and an annual Crab Nebula observing campaign, RHESSI observes the full Sun continuously.

The primary science data are returned in event data packets whose contents include the time, energy and detector-segment identification for each detected photon. Aspect data are provided with sufficient time resolution that the instantaneous aspect associated with each detected event can be inferred. Monitor rates with lower time resolution are also available to provide an overview of detector performance.

Data acquisition averages about 2 GB per day and is based on a store-and-dump system using a 4 GB on-board memory. There are typically ~11 prescheduled downlink passes per day divided between the Berkeley Ground Station (BGS) and NASA Wallops Ground Station (WGS) with additional telemetry support provided by ground stations at Weilheim, Germany, and Santiago, Chile (AGO).

Because the RHESSI data is photon-based, analysts can (iteratively) choose the optimum time, spectral and spatial resolution and coverage best suited to his/her specific science objectives and the flare(s) in question. Such decisions can therefore be made during the analysis phase, as opposed to the implementation or operations phase of the mission. This provides a powerful degree of flexibility, the value of which has been well proven over the years. Preserving this flexibility is a primary driver for the RHESSI analysis software and data strategy.

3.2 Current RHESSI Data Archive, Software and Documentation

3.2.1 RHESSI Data Archive

The current RHESSI data archive contains the full Level-0 telemetry data, the RHESSI flare list, and a number of catalog or quicklook data products (QLPs) including mission-long light curves, flare spectra and images, and summaries of housekeeping data. The full archive (~9 TB as of March 2015) resides on servers at SSL and is automatically mirrored at GSFC and the HESSI European Data Center (HEDC) at FHNW, Windisch, Switzerland. It is online and accessible by anyone. The online archive, including metadata, quicklook products and engineering data, is updated automatically, typically within an hour of receipt at the MOC, by converting the received telemetry to FITS files and adding it to the online dataset where it is available for scientific analysis.

The Level-0 data files contain the full raw telemetry data in packed time-ordered format. All of the quicklook product generation and detailed analyses of RHESSI data start with the Level-0 files. These files contain science data ('photon-tagged events' that encode the detector ID, arrival time, and energy for each detector count), monitor rates, solar aspect data and housekeeping data. Even though these files are in a standard FITS format, they are meaningful only through the RHESSI SSW software due both to the complex data packing scheme and that images must be deconvolved from the instantaneous aspect and photon arrival times. Calibration information needed to interpret these data is distributed with and accessed by the analysis software. The entire Level-0 database is currently being stored in a deep archive at the NSSDC with a latency of a few months. As of March 2015, it contains data through December 2014.

The QLPs include a flare list containing the time, duration, size, location, and other parameters and flags for the >100,000 events automatically identified in the RHESSI data. The full flare list is available in the archive (and viewable through a browser) as one large text file. In addition, monthly flare list files are stored in FITS format, as well as text files for easy direct viewing. The RHESSI software reads the FITS files, automatically merging the monthly files, and provides options for selecting analysis time intervals based on flare parameters.

The QLPs allow the RHESSI observations to be surveyed. Using the same software used for higher-level analysis, they are created automatically from the Level-0 data both as FITS files and browser-viewable image formats such as GIF, PNG, or text files.

The QLP FITS files include daily observing summary data from which analysts can quickly generate plots of light curves in 9 standard energy bands. These files also contain spacecraft ephemeris and pointing information and the modulation variance. For most flares, the QLPs also include representative spectra and images that are intended as a starting point for most analyses. (Detailed analysis of a flare is done using the Level-0 data, where the user can select the times, energies, detectors, etc. that are best suited to the scientific objectives and the event under study.) The prepared plots can be viewed directly by accessing the archive metadata directories, or more easily through the versatile RHESSI Browser at http://sprg.ssl.berkeley.edu/~tohban/browser/. This allows users to display more than 20 different products including light curves, images, spectra, monitor rates, and comparisons with GOES.

In addition, RHESSI housekeeping data for the entire mission are available in the archive and can be accessed at http://hessi.ssl.berkeley.edu/hessidata/metadata/hsi_1day_sohdata/. Text files and GIF plots provide a record of the average daily values for ~100 state-of-health parameters including spacecraft bus voltages and currents, imager aspect sensor parameters, spectrometer cryocooler power and temperature, and more.

Access to the data archive is almost transparent. Users located at a site hosting the full data archive (Goddard, Berkeley, or FHNW) share the data directories from a local file server. Remote users set a feature in the software to enable network searching and copying of files from an archive to their own computer. In either case, the software automatically determines the files needed for the selected time interval and after either sharing or copying them, reads them and retrieves the requested data for processing.

3.2.2 Software

Almost all the RHESSI software package (Schwartz et al. 2002) is written in Interactive Data Language (IDL, licensed from Exelis Visual Information Solutions). It contains all procedures necessary to read and unpack the FITS data files, prepare and plot light curves, reconstruct images, and accumulate, display, and analyze spectra. Analysis procedures can be invoked from a combination of the IDL command line, user-generated scripts building on these commands, or a graphical user interface (GUI) that forms a user-friendly shell around the basic analysis routines. The software is fully compatible with Linux, Mac OS X, and Windows operating systems and is freely available as part of the Solar Software (SSW) tree.

The RHESSI data analysis software is a robust object-oriented system that allows any analyst with access to Level-0 files, calibration data, and the QLPs to generate and analyze RHESSI lightcurves, spectra, and images. Higher level capabilities include generating image cubes and movies of images at multiple time and energy intervals, background subtraction, feature-based imaging spectroscopy, and performing joint analysis of many different observations of the same events by other observatories. The software can be downloaded to any user's computer as part of the Solar Software (SSW) installation following instructions provided on the RHESSI web site. The only requirement is that the user has a license for IDL version 6.2 or higher.

3.2.3 Documentation and Support

Extensive documentation describing the mission, instrumentation, analysis techniques, software, and data access can be found via a single RHESSI web site: http://hesperia.gsfc.nasa.gov/rhessi/. Support personnel at SSL and GSFC are also available to provide guidance as needed in using the software and interpreting the results.

The extensive online RHESSI documentation provides both background and explanatory material on the RHESSI mission, as well as instructions for almost every aspect of the software, from installation through use of the objects and the GUI. Detailed descriptions of every data product and warnings about misinterpreting data are available. There are 'First Steps' instructions for imaging and spectroscopy to guide users through sample GUI sessions and explanations of the use of the objects. A software FAQ is available to provide solutions to common questions or problems.

The dedicated email address - rhessi-help@lists.nasa.gov - is available for reporting RHESSI software bug reports and questions. It is monitored by one of the team members and any queries are answered promptly either by the monitor or by other core members of the RHESSI group to address more specialized issues. All bug reports and their solutions are archived for user access.

3.3 Plans for the RHESSI Legacy Archive

3.3.1 Introduction

The legacy archive will include the data products, software, and documentation discussed above, as well as secondary databases of scientific interest and several new data products under development, all of which are described in more detail below. This section emphasizes the tasks related to adapting and enhancing those data sets to make them effective with a reduced (or eliminated) level of support from the instrument team.

3.3.2 Data Products

3.3.2.1 *Quicklook Products*

The Level-1 data products serve the needs of those requiring a convenient overview of the data and basic X-ray data products (light curves, representative images, and spectra, etc.). The catalog data to be archived for post-mission use are identical in form and content to that described in Section 3.2.

3.3.2.2 *Level-0 Data*

To meet the needs of solar and non-solar analyses without compromising the full potential of the data, the Level-0 data as described in Section 3.2 will be made part of the Resident and Final Archives, along with the corresponding analysis tools and documentation.

3.3.2.3 *Visibility Data*

As discussed above, a key driver of the RHESSI analysis approach has been to maintain the ability of the user to flexibly choose the time, spatial, and energy resolution and range that best matches their scientific objectives and events under study. To achieve this, however, it is necessary for users to start from Level-0 data and use the RHESSI-specific IDL software package. While this continues to be effective, it may become more problematic without the occasional one-on-one interaction with experienced users. For the long-term, therefore, it is desirable to identify a way by which most of the flexibility can be maintained without necessarily resorting to the Level-0 data.

Visibilities provide a natural way to accomplish this. A RHESSI visibility is a fully calibrated measurement of a specific Fourier component of the source spatial distribution for a given time interval and (count) energy bin. In radio parlance, each visibility corresponds to a single uv point. Such visibilities are a direct output of RHESSI's time-modulated measurements of X-ray flux. While RHESSI's 'normal' imaging algorithms bypass the explicit calculation of visibilities, the object-oriented software to convert RHESSI's photon-based data to calibrated visibilities has been incorporated into the RHESSI software package and an increasing fraction of papers now use visibility-based analyses. Furthermore, some capabilities, such as the generation of electron-images, can only be generated through visibilities. In addition to the efforts of the RHESSI PI team, the High Energy Solar Physics in Europe (HESPE) program, funded by ESA, is generating and archiving visibility-based data for long-term use.

While making some compromises in time and/or energy resolution, the use of visibilities has several distinct advantages.

- Visibilities are an inherently compact representation of the RHESSI data, preserving its key information content in a form that is typically ~2 orders of magnitude more compact than photon-based data.
- Unlike reconstructed images, visibilities are a *linear* representation of the data so they can be combined across different time/energy ranges to meet the user's needs.
- For each detected energy range, visibilities are fully calibrated, thus relieving the user of instrument-specific calibration tasks.
- Visibilities provide a more robust method of determining accurate source sizes as compared to inspection of reconstructed images.
- Measured visibilities include well-determined statistical errors whose propagation supports quantitative assessment of the significance of derived results.
- Calibrated X-ray visibilities have the identical significance as visibilities obtained from radio interferometers. Thus, a set of X-ray visibilities can be manipulated and converted to an image using any of several existing radio interferometer analysis packages, independent of RHESSI-specific software.

These considerations suggest that, in addition to the catalog and Level-0 data products discussed above, the inclusion of an extensive set of calibrated flare X-ray visibility data would provide a flexible option to meet the needs of users well into the future.

To do so, the following tasks remain to be accomplished:

- While the basic software for visibility calculation has been implemented, there are several important areas in which it needs to be refined.
- Automated algorithms need to be developed to optimally choose statistically significant time and energy intervals within which to calculate visibilities. Such algorithms are currently under development for other missions (e.g., STIX on Solar Orbiter) and can be re-parameterized for the present purpose.
- The suitability of FITS as the optimum archive format for the calculated visibilities to support long-term use and compatibility with radio software packages needs to be confirmed.
- Scripts need to be developed and executed to apply these algorithms to the mission-long RHESSI data set and to convert the visibilities to the archive format.
- More extensive documentation needs to be developed for use by unsupported users in the Resident and/or Final Archive phases.

3.3.2.4 *Level-2 Data Products*

We are in the process of adding three science-ready event-oriented databases for photon images, spectra and lightcurves. This effort has been funded under the data environment enhancement program. The FITS files created will be readable in any scientific software environment. For each flare, we will include:

- High quality photon flux images made using the pixon algorithm in our standard energy bands at a cadence dictated by the data rates. Using about 10,000 counts per sub-collimator these images will show the principal flaring structures in the corona at low energy, and in the chromosphere at higher energy. While not suitable for imaging spectroscopy or high time-resolution studies, they will be extremely useful in correlative studies at non X-ray wavelengths and will require no further RHESSI-specific analysis. Recent improvements to the pixon routine have increased its performance by a factor of 3–10.
- Photon lightcurves made in our standard energy bands up to 300 keV. These data will be background-subtracted allowing for spectral deconvolution from counts to photons. While it won't be possible to remove all instrument artifacts, these lightcurves will be suitable for immediate display and comparison with other wavelengths.
- Photon spectra up to 300 keV will be produced on a time-scale commensurate with the images produced in the nonthermal energy range. Count spectra and estimated background spectra will also be available, as well as any needed detector responses for use with our spectral analysis package

3.3.2.5 *Other RHESSI Databases*

The additional databases described in this section have the common feature that the data are distributed throughout the multi-terabyte Level-0 database. For the convenience of non-experts, we extract and process the relevant material into compact, standalone databases for subsequent analysis.

Solar Radius Data

In addition to providing essential pitch and yaw aspect data for X-ray image reconstruction, the Solar Aspect System (SAS) data constitute a unique database of highly precise measurements of solar radii (Fivian et al. 2005) with applications to fundamental solar properties such as solar oblateness and p-modes,. The dataset comprises ~100 radius measurements per second (totaling $>3 \times 10^{10}$ measurements to date), each with a statistical error of a few tens of milli-arcseconds.

SAS data require elaborate analyses to remove diverse systematic effects in order to obtain their inherent precision. As a result, these data benefit from the creation of secondary databases, both to isolate the SAS data set itself and to reflect the application of internally derived calibration parameters. Although a preliminary version of such a database exists, for the legacy archive, it will need to be finalized and fully documented, a task that will require ~ 1 man-year.

Roll Aspect Database

We are creating a Roll Aspect Solution database for the entire mission. Currently, the software determines the instantaneous roll solution based on the PMTRAS (Photomultiplier Roll Aspect Sensor) data that are included in the Level-0 files. We estimate that this software works successfully ~98% of the time based on the number of flare locations at implausible high latitudes. We want to reduce that error rate, particularly as the availability of expert assistance becomes lessened as our staffing levels decrease. Therefore, we will extracted the entire set of PMTRAS data and will use that to create a robust roll solution database.

Radiation Studies

Mission-long examination of nuclear radiation data is useful for studies of galactic Al^{26}, galactic positron annihilation, novae, and quiet-Sun 2.2 MeV neutron-capture-line emission. As the mission progresses a database of accumulated 1-minute spectra from the rear detector segments is being amassed and will be added to the archive. Documentation will be generated during the transition to the Resident Archive phase.

Terrestrial Gamma-Ray Flashes (TGFs)

A catalog of transient events identified by an automated TGF triggering algorithm is being assembled as the mission progresses. During the Resident Archive phase, this will be finalized and documented for use as part of the Final Archive.

Spectrometer Status Database

We are collecting complete records of the status of the spectrometer, including detector segmentation and threshold level changes resulting from radiation damage and detector annealing. These augment the existing calibration files and will facilitate detector selection in both spectroscopy and imaging analyses.

3.3.2.6 *SDO/AIA Cutout Image Database*

SDO/AIA cutout image FITS files and movies are generated for every RHESSI flare observed after Sept. 2010. The cutouts are 300 arcsec squares at the highest cadence for all the AIA channels running from a few minutes before the start of the RHESSI flare though a few minutes after the end. These movies are linked from the RHESSI Browser, and the FITS files are accessible through the Synoptic Data Archive.

3.3.3 Analysis Tools for Level-0 data

The basis for all legacy archive analysis tools is the IDL-based, SSW-distributed software that has been routinely used during the mission for the creation and interpretation of scientific data products. To maintain the integrity of the software within the dynamic SSW environment we will archive a snapshot of all the elements of the SSW tree necessary for RHESSI analysis, specifically the GEN, HESSI, X-RAY, and SPEX branches. This will ensure that the software that was working at the end of mission will continue to work into the future.

With successive cycles of progressive radiation damage and annealing, the RHESSI detector response has changed during the course of the mission. To accommodate this, detector response parameters in the SSW distribution have been periodically updated so that, transparent to the user, the appropriate time-dependent calibration parameters are applied for each analysis. In preparation of the legacy archive, it will be necessary to ensure that this calibration has been updated as required to cover the full mission.

3.3.4 Documentation

While an extensive range of documentation is available via the RHESSI website, it needs to be carefully reviewed so that it can effectively serve its purpose during the Resident and Final Archive phases with reduced (or absent) one-on-one support. Specifically, obsolete or conflicting material needs to be identified and updated or removed, perceived gaps need to be identified and a robust stand-alone guide to the material generated. While on-going at a low level, this task will be completed during the Resident Archive phase, requiring an estimated 2–4 months of effort by a combination of experienced RHESSI personnel. Additional emphasis will be placed on introductory material, indexing, and consolidating distributed information to provide a mission-long overview and time-ordered log of RHESSI performance.

3.3.5 Distribution

During the year after the end of the mission, RHESSI data products will continue to be accessible from servers at SSL and GSFC (and possibly through the Swiss-funded mirror site at

FHNW). The archive will then be transitioned to the Resident Archive at the Solar Data Analysis Center (SDAC) at Goddard. The legacy archive will be hosted by the National Space Science Data Center (NSSDC) at Goddard.

Access of RHESSI data through the VSO involves three approaches. The first is to include the Catalog data into the VSO. This will make it possible on one hand, to display quick-look products in VSO query results, and on the other, to download pre-calculated images or image cubes for comparison with data sets from other instruments. This requires no RHESSI-specific software.

The second approach is to implement event-based queries, i.e., queries based on the flare list and the observing summary in addition to queries based on a time range. This means that the RHESSI archive can be searched, for example, for flares of specific characteristics such as size, duration, or location on the limb.

The third approach is to provide an indexed database of flare visibilities, a subset of which can be identified and provided in response to user time, energy, location or other criteria. These can be manipulated and/or converted to images at the user's institution using either a simplified subset of IDL software or by external radio interferometric packages such as MIRIAD (Multichannel Image Reconstruction, Image Analysis and Display). To allow correct inclusion of the RHESSI data into the VSO, the Catalog data will be annotated in the FITS headers with keywords defined by the SPASE consortium. Adopting SPASE keywords will guarantee that SPASE data analysis programs can use RHESSI Catalog data. The visibility data will also be described by SPASE-compatible keywords. The Level-0 database, however, does not need to be SPASE annotated, as it requires the RHESSI-specific software to generate science-ready products.

3.3.6 Schedule

Estimates of the effort required to go from the end of mission to complete documentation and delivery of the legacy archive are as follows: Catalog and Level-0 data preparation: 0.1 FTE; visibility data software development, validation and database generation 2 FTE, solar radius data 1 FTE; radiation studies: 0.2 FTE; TGF database: 0.2 FTE; analysis tools, 0.2 FTE; documentation 0.4 FTE, distribution, 0.5 FTE; for a total of 4 to 5 FTE. These tasks should be completed within an elapsed time of ~2 years from the end of mission using an appropriate mix of experienced RHESSI personnel. This suggests that the cost of the final archiving effort will be in the range of $0.8M to $1M.

3.4 References

Fivian, M. D., Hudson, H. S., & Lin., R. P. 2005 in *Proc 11th European Solar Physics Meeting*, ESA SP- 600, 41

Lin, R. P., et al. 2002, Solar Phys., 210, 3

Schwartz, R. A., et al. 2002, Solar Phys., 210, 165

ACRONYM LIST

A&A	Astronomy & Astrophysics Journal
AAS	American Astronomical Society
ACE	Advanced Composition Explorer
ACS	Attitude Control System
AESP	Aerospace Education Services Program
AGILE	Italian Space Agency gamma-ray mission
AGO	Santiago ground station
AGU	American Geophysical Union
AIA	Atmospheric Imaging Assembly on SDO
AIM	Aeronomy of Ice in the Mesosphere
AISES	American Indian Science and Engineer Society
ALMA	Atacama Large Millimeter/submillimeter Array
ApJ	Astrophysical Journal
ARTEMIS	Acceleration, Reconnection, Turbulence and Electrodynamics of the Moon's Interaction with the Sun
ASIM	Atmosphere-Space Interactions Monitor
ATS	Absolute Time Sequence
AU	Astronomical Unit
BATSE	Burst and Transient Source Experiment on CGRO
BBSO	Big Bear Solar Observatory
BGO	Bismuth Germinate used as a scintillation detector
BGS	Berkeley Ground Station
BPSK	Binary Phase Shift Keying
Cal Day	Open House at the Space Sciences Laboratory at the University of California, Berkeley
CAST	CERN Axion Solar Telescope
CCD	Charge Coupled Device
C&DH	Command and Data Handling
CD-ROM	Compact Disk – Read Only Memory
CDS	Coronal Diagnostic Spectrometer on SOHO
CERN	European Organization for Nuclear Research
CHIPS	Cosmic Hot Interstellar Plasma Spectrometer
CGRO	Compton Gamma Ray Observatory
CINEMA	Cubesat for Ion, Neutral, Electron, & Magnetic fields
CLI	Command Line Interface
CME	Coronal Mass Ejection
CoMP	Coronal Multi-channel Polarimeter
COMPTEL	Compton Telescope on CGRO
CoP	Community of Practice
COR-1	Inner Coronagraph of STEREO SECCHI instrument
COR-2	Outer Coronagraph of STEREO SECCHI instrument
COSPAR	COmmittee on SPAce Research
CP	Charge conjugation/Parity
CRISP	Crisp Imaging Spectro-polarimeter in Sweden
CSE@SSL	Center for Science Education at Space Sciences Laboratory
CSRH	Chinese spectro-radioheliograph
CSTA	California Science Teachers Association
DEM	Differential Emission Measure
DKIST	Daniel K. Inouye Solar Telescope (formerly the Advanced Technology Solar Telescope, ATST)
DSCOVR	Deep Space Climate Observatory (formerly Triana)
DL	Double Layer
DLR	Weilheim ground station
DST	Dunn Solar Telescope National
EGRET	Energetic Gamma Ray Experiment Telescope on CGRO

ERC	Educator Resource Center
EEPROM	Electrically Erasable Programmable Read-Only Memory
EIT	Extreme Ultraviolet Imaging Telescope on SOHO
EIS	EUV imaging spectrograph on Hinode
EOVSA	Expanded Owens Valley Solar Array
E/PO	Education and Public Outreach
ETH(Z)	Eidgenossische Technische Hochschule (Zentrum), Zurich, Switzerland
EUV	Extreme UltraViolet
EUVI	Extreme UltraViolet Imager on STEREO
EVA	Extra-Vehicular Activity
EVE	Extreme Ultraviolet Variability Experiment on SDO
EVLA	Expanded Very Large Array
FAST	Fast Auroral SnapshoT
FAQ	Frequently Asked Questions
FDC	Flight Dynamics Center
Fermi	Fermi Gamma-ray Space Telescope (formerly GLAST)
FFT	Fast Fourier Transform
FHNW	Fachhochschule Nordwestschweiz - University of Applied Sciences and Arts, Northwestern Switzerland
FIP	First Ionization Potential
Firefly	NASA microsatellite for studying TGFs
FITS	Flexible Image Transport System
FORMOSAT-2	Earth Observation Satellite
FOT	Flight Operations Team
FoV	Field of View
FPI	Fabry-Perot Interferometer
FTE	Full time Equivalent
FWHM	Full Width at Half Maximum
GB	Gigabytes
GBM	Gamma-ray Burst Monitor on Fermi
GDS	Ground Data System
Ge	Germanium
GeD	Germanium Detector
GEMS	Great Explorations in Math and Science
GEONS	Geomagnetic Event Observation Network by Students
GIF	Graphics Interchange Format
GLAST	Gamma-ray Large Area Space Telescope (now Fermi)
GLE	Ground Level Event
GOES	Geostationary Operational Environmental Satellite
GRB	Gamma Ray Burst
GREGOR	Gregory-type German 1.5 m solar telescope on Tenerife
GRIS	GREGOR Infrared Spectrograph
GRS	Gamma Ray Spectrometer
GSFC	Goddard Space Flight Center
G/T	Antenna gain to noise temperature ratio
GUI	Graphical User Interface
HD	Heliophysics Division
HEA	Heliophysics Educator Ambassadors
HEAD	High Energy Astrophysics Division
HE CoP	Heliophysics Educator Community of Practice
HEDC	HESSI European Data Center
HEPAD	High Energy Proton and Alpha Particle Detector on GOES
HESPE	High Energy Solar Physics in Europe
HGO	Heliophysics Great Observatory
Hinode	Japanese solar satellite - formerly Solar-B
HMI	Helioseismic and Magnetic Imager on SDO

HP	Heliophysics
HSO	Heliophysics System Observatory
HST	Hubble Space Telescope
HXR	Hard X-ray
HXT	Hard X-ray Telescope on Yohkoh
IBIS	Interferometric BIdimensional Spectropolarimeter (installed at Dunn Solar Telescope)
IDL	Interactive Data Language
IDPU	Instrument Data Processing Unit
IGES	Institute for Global Environmental Strategies
IMPACT	In-situ Measurements of Particles and CME Transients on STEREO
IPM	Interplanetary Medium
IPN	Interplanetary Network
IRIS	Interface Region Imaging Spectrograph (Small Explorer mission)
ISSI	International Space Science Institute
ISUAL	Imager of Sprites and Upper Atmospheric Lightnings on FORMOSAT-2
ITOS	Integrated Test and Operations System
JGR	Journal of Geophysical Research
KSC	Kennedy Space Center
LASCO	Large Angle and Spectrometric Coronagraph on SOHO
LAT	Large Area Telescope on Fermi
LDGRF	Long Duration Gamma-Ray Flares
LHCP	Left-Handed Circular Polarization
LHS	Lawrence Hall of Science
LOFAR	Low-Frequency Array (Netherlands)
LSEP	Large SEP event
mas	milli-arcsecond
MB	Megabytes
MDI	Michelson Doppler Imager on SOHO
MESSENGER	MErcury Surface, Space ENvironment, GEochemistry, and Ranging
MHD	Magnetohydrodynamics
MILA	Merritt Island ground station
MOC	Mission Operations Center
MO&DA	Mission Operations and Data Analysis
MOU	Memorandum of Understanding
MPS	Mission Planning System
MWA	Murchison Widefield Array
NaI	Sodium Iodide used as a scintillation particle detector
NASA	National Aeronautics and Space Administration
NCAR	National Center for Atmospheric Research
NJIT	New Jersey Institute of Technology
NLFF	Non-Linear Force-Free (magnetic field)
NRH	Nancay Radioheliograph
NSO	National Solar Observatory
NSSDC	National Space Science Data Center
NSTA	National Science Teacher Association
NuSTAR	Nuclear Spectroscopic Telescope Array - orbiting telescopes to focus HXRs
OCA	Orbital Carrier Aircraft
OEPM	NASA's Office of Education Performance Measurement
OIG	Orbital Information Group
OVSA	Owens Valley Solar Array
PD	Professional Development
PIC	Particle In Cell
PMTRAS	Photomultiplier Tube Roll Angle System on RHESSI
PNG	Portable Network Graphics
POEMAS	POlarization Emission of Millimeter Activity at the Sun in Argentina
POLIS	Polarimetric Littrow Spectrograph

PSG	Prioritized Science Goal
PSLA	Project Service Level Agreement
QLP	Quick Look data Product
QPP	Quasi-Periodic Pulsations
RAD6000	Radiation-hardened single board computer used on spacecraft
RAID	Redundant Array of Inexpensive Disks
RAS	Roll Angle System
RF	Radio Frequency
RHCP	Right-Handed Circular Polarization
RHD	Radiative Hydrodynamic
RHESSI	Reuven Ramaty High Energy Solar Spectroscopic Imager
RMC	Rotating Modulation Collimator
SAA	South Atlantic Anomaly
SACNAS	Society for Advancement of Chicanos and Native Americans in Science
SAMPEX	Solar Anomalous and Magnetospheric Particle Explorer
SAS	Solar Aspect System on RHESSI
SAX	Solar Assembly for X-rays on MESSENGER
SatTrack	Satellite Tracking software
SDAC	Solar Data Analysis Center
SDO	Solar Dynamics Observatory
SECCHI	Sun Earth Connection Coronal and Heliospheric Investigation on STEREO
SECEF	Sun Earth Connection Education Forum
SED	Sun-Earth Day
SEE	Solar Eruptive Event
SEGway	Science Education Gateway
SEP	Solar Energetic Particles
SEPT	Solar Electron Proton Telescope on STEREO / IMPACT
SERS	Spacecraft Emergency Response System
SGR	Soft Gamma Repeater
SHH	Soft, Hard, Harder –HXR spectral evolution
SHS	Soft, Hard, Soft – HXR spectral evolution
SMD	Science Mission Directorate
SMEX	NASA's Small Explorer Program
SMM	Solar Maximum Mission
SOC	Science Operations Center
SOH	State-Of-Health
SOHO	Solar and Heliophysics Observatory
SORCE	Solar Radiation and Climate Experiment
SOT	Solar Optical Telescope on Hinode
SOXS	Solar X-ray Spectrometer
SPASE	Space Physics Archive Search and Extract
SPD	Solar Physics Division
SSL	Space Sciences Laboratory (University of California, Berkeley)
SSMO	Space Science Mission Operations
SSR	Solid State Recorder
SSRT	Siberian Solar Radio Telescope
SST	Swedish Solar Telescope
SSW	SolarSoftware
STE	Suprathermal Electron Telescope on STEREO / IMPACT
STEM	Science, Technology, Engineering, and Math
STEREO	Solar TErestrial RElations Observatory
STIX	Spectrometer Telescope for Imaging X-rays on Solar Orbiter
SUMER	Solar Ultraviolet Measurements of Emitted Radiation on SOHO
SWAC	Space Weather Action Center
SXI	Soft X-ray Imager
SXR	Soft X-ray

TARANIS	Tool for the Analysis of RAdiations from lightNIngs and Sprites
TB	Terabytes
TGF	Terrestrial Gamma-ray Flash
THEMIS	Time History of Events and Macroscale Interactions during Substorms
TRACE	Transition Region and Coronal Explorer
UCB	University of California at Berkeley
UT	Universal Time
VCn	Virtual Channel n
VLF	Very Low Frequency (radio waves)
VSO	Virtual Solar Observatory
VxWorks	A real-time operating system
WAVES	Radio and Plasma Wave Investigation on the WIND spacecraft
WebEx	Web conferencing application
WGS	Wallops Ground Station
WIND	Spacecraft for long-term solar wind measurements
WISE	Wide Field Infrared Survey Explorer
WL	White-Light
WLF	White-Light Flare
WWLLN	World Wide Lightning Location Network
WYE	Work Year Estimate
XRT	X-Ray Telescope on Hinode
Yohkoh	Japanese Solar Satellite